

## Impact of a New Radiation Package, McRad, in the ECMWF Integrated Forecasting System

J.-J. MORCRETTE

*European Centre for Medium-Range Weather Forecasts, Reading, United Kingdom*

H. W. BARKER

*Environment Canada, Toronto, Ontario, Canada*

J. N. S. COLE

*Department of Earth and Ocean Sciences, The University of British Columbia, Vancouver, British Columbia, Canada*

M. J. IACONO

*Atmospheric and Environmental Research, Inc., Lexington, Massachusetts*

R. PINCUS

*NOAA/Earth Systems Research Laboratory/Physical Science Division, and Cooperative Institute for Research in Environmental Sciences Climate Diagnostics Center, University of Colorado, Boulder, Colorado*

(Manuscript received 30 August 2007, in final form 26 March 2008)

### ABSTRACT

A new radiation package, "McRad," has become operational with cycle 32R2 of the Integrated Forecasting System (IFS) of the European Centre for Medium-Range Weather Forecasts (ECMWF). McRad includes an improved description of the land surface albedo from Moderate Resolution Imaging Spectroradiometer (MODIS) observations, the Monte Carlo independent column approximation treatment of the radiative transfer in clouds, and the Rapid Radiative Transfer Model shortwave scheme. The impact of McRad on year-long simulations at  $T_L159L91$  and higher-resolution 10-day forecasts is then documented. McRad is shown to benefit the representation of most parameters over both shorter and longer time scales, relative to the previous operational version of the radiative transfer schemes. At all resolutions, McRad improves the representation of the cloud–radiation interactions, particularly in the tropical regions, with improved temperature and wind objective scores through a reduction of some systematic errors in the position of tropical convection as a result of a change in the overall distribution of diabatic heating over the vertical plane, inducing a geographical redistribution of the centers of convection. Although smaller, the improvement is also seen in the rmse of geopotential in the Northern and Southern Hemispheres and over Europe. Given the importance of cloudiness in modulating the radiative fluxes, the sensitivity of the model to cloud overlap assumption (COA) is also addressed, with emphasis on the flexibility that is inherent to this new RT approach when dealing with COA. The sensitivity of the forecasts to the space interpolation that is required to efficiently address the high computational cost of the RT parameterization is also revisited. A reduction of the radiation grid for the Ensemble Prediction System is shown to be of little impact on the scores while reducing the computational cost of the radiation computations. McRad is also shown to decrease the cold bias in ocean surface temperature in climate integrations with a coupled ocean system.

---

*Corresponding author address:* Dr. Jean-Jacques Morcrette, ECMWF, Shinfield Park, Reading RG2 9AX, United Kingdom.  
E-mail: morcrette@ecmwf.int

DOI: 10.1175/2008MWR2363.1

© 2008 American Meteorological Society

TABLE 1. Major changes in the representation of radiative transfer in the ECMWF forecasting system.

Cycle	Date of implementation	Description
SPM32	2 May 1989	RT schemes from University of Lille
SPM46	1 Feb 1993	Optical properties for ice and mixed-phase clouds
IFS 14R3	13 Feb 1996	Revised LW and SW absorption coefficients from 1992 High-Resolution Transmission Model (HITRAN-92)
IFS 16R2	15 May 1997	Voigt profile in longwave RT scheme
IFS 16R4	27 Aug 1997	Revised ocean albedo from ERBE
IFS 18R3	16 Dec 1997	Revised LW and SW absorption coefficients from HITRAN-96
IFS 18R5	1 Apr 1998	Seasonal land albedo from ERBE
IFS 22R3	27 Jun 2000	RRTM <sub>LW</sub> as longwave RT scheme, shortwave RT scheme with 4 spectral intervals
IFS 23R4	12 Jun 2001	Hourly, instead of 3-hourly, calls to RT code during data assimilation cycle
IFS 25R1	9 Apr 2002	Shortwave RT scheme with 6 spectral intervals
IFS 26R3	7 Oct 2003	New aerosol climatology adapted from Tegen et al. (1997)
IFS 28R3	28 Sep 2004	Radiation called hourly in high-resolution forecasts
IFS 32R2	5 Jun 2007	McICA approach to RT with RRTM <sub>LW</sub> and RRTM <sub>SW</sub> , revised cloud optical properties, MODIS-derived land albedo

## 1. Introduction

Although it has always been recognized that an accurate representation of the radiative transfer (RT) is a precondition for a good climate simulation, a similar requirement for weather forecasts was thought in the 1970s to be a luxury, given the long time scale generally ascribed to radiative processes. Table 1 gives the timeline of the major changes affecting the representation of the radiative transfer in the European Centre for Medium-Range Weather Forecasts (ECMWF) model over the last 20 years. ECMWF, with its 10-day forecasts, was, from its inception, one of the very first weather forecast centers in which emphasis was put on having a reasonably accurate radiative transfer parameterization, interactive with humidity and cloudiness (Geleyn, 1977; Geleyn and Hollingsworth, 1979).

Even if by today's standards these first versions of the ECMWF radiation codes were not free from systematic errors, they had already provided interactivity with the temperature, with the water vapor, and then, a few years later, with the distribution of the fractional cover and optical thickness of clouds provided by the diagnostic cloud scheme (Slingo 1987). These first versions served their purpose with a fair description of the equator–Pole gradient in the deposition of radiative energy and of the vertical distribution of the total radiative heating.

At the end of the 1980s, the Intercomparison of Radiation Codes for Climate Models (ICRCCMs; Fouquart et al. 1991; see special issue of *Journal of Geophysical Research*, 1991, Vol. 96D, No. 5) provided the first opportunity to compare in a systematic way the results of general circulation model (GCM)-type radiation schemes with line-by-line (LBL) models of the

infrared radiation transfer and to document their successes and failures. A more extensive description of the characteristics of the early ECMWF schemes can be found in Morcrette (1991), together with a description of the RT schemes that were originally developed at the University of Lille, which replaced these early schemes in May 1989. This replacement followed an assessment of the systematic errors in the forecast model that were linked to the representation of the radiative processes provided by these early schemes (Morcrette 1990). In the following years, cloud optical properties were revised, following the availability of new parameterizations (Morcrette 1993).

At the end of the 1990s, following the developments in line-by-line RT models and the emergence of much more accurate measurements of the surface radiation fields and the temperature and water vapor profiles [mainly as part of the Atmospheric Radiation Measurement (ARM) Program of the U.S. Department of Energy but also part of the dedicated surface radiation network (SURFRAD) in the United States and the Baseline Surface Radiation Network (BSRN)], it became possible to validate the clear-sky radiation fields that were computed by a GCM-type RT scheme to within a few watts per square meter in the longwave (LW) and to within 10–15 W m<sup>-2</sup> in the shortwave (SW) part of the spectrum.

In 2000, the Rapid Radiative Transfer Model (RRTM), the longwave RT scheme (Mlawer et al. 1997) developed at Atmospheric and Environmental Research, Inc., from the line-by-line RT model (LBLRTM; Clough et al. 1992; Clough and Iacono 1995) was adapted to the ECMWF computer environment, extensively tested (Morcrette et al. 1998), and adopted as the operational longwave RT scheme (Morcrette et al.

2001). In parallel, following comparisons with some of the surface observations discussed above (Morcrette 2002a,b), revisions were made to the shortwave radiation scheme (extended from 2 to 4 spectral intervals in June 2000 and then to 6 spectral intervals in April 2002).

Despite the improvements brought to the representation of the clear-sky radiative fluxes by these revised/new schemes, the handling of cloudiness kept following an approach that was originally introduced 20 yr earlier by Geleyn and Hollingsworth (1979). Various sensitivity studies (e.g., Morcrette and Fouquart 1986; Barker et al. 1999; Morcrette and Jakob 2000) had shown the huge impact that a change in cloud overlap assumption (COA) usually brings to the instantaneous radiative fluxes at the boundaries of the atmosphere and radiative heating rate profiles. Also, ground-based cloud radar measurements at a midlatitude location (Hogan and Illingworth 2000, 2003) were showing that the maximum-random COA generally used in GCM-type RT schemes (Barker et al. 2003) did not provide enough decorrelation, even for cloud layers distributed continuously over the vertical (i.e., the observed cloud layers appear more randomly distributed on the vertical than model cloud layers distributed according to the maximum-random overlap). These measurements, repeated at other locations as part of the ARM Program, confirmed these early conclusions.

Unfortunately, the GCM-type RT schemes prevalent at the time could not be easily made flexible enough to accommodate these observationally based cloud overlap distributions. This deficiency together with concerns—about the role of the spatial inhomogeneity in the distribution of the condensed water within a layer [first addressed by Cahalan et al. (1994) and then by a number of authors including Barker et al. (1999, 2003, 2002)] and about upgrading the gaseous absorption coefficients following the release of a new version of the spectroscopic database—were the reason for the adoption of a new approach to radiation transfer.

This paper documents the various elements included in the new radiation package that were used in all configurations of the ECMWF Integrated Forecasting System (IFS). Also a new radiation package, “McRad,” will be the radiation scheme used in a future reanalysis. Consequently, this paper is aimed at documenting its main impact on the various configurations of the model.

## 2. Description of a new radiation package for the ECMWF Integrated Forecast System

As part of the modifications to create the model library that became operational on 5 June 2007 [the so-

called cycle 32 release 2 (CY32R2)], the radiation transfer package was modified along three lines.

- 1) The spectrally flat land surface albedo derived from Earth Radiation Budget Experiment (ERBE) satellite measurements was replaced by a land surface albedo with four components derived from Moderate Resolution Imaging Spectroradiometer (MODIS) satellite measurements: albedo for direct and diffuse radiation were given for the two spectral intervals on both sides of  $0.7 \mu\text{m}$ .
- 2) The radiation transfer in clouds is treated following the Monte Carlo Independent Column Approximation (McICA).
- 3) The shortwave radiation scheme is based on the RRTM, originally developed by Clough et al. (2005) and Iacono et al. (2008), making it fully consistent with the RRTM longwave code, which has been operational at ECMWF since June 2000.

In the following, this new radiation package is referred to as McRad. The resolution of the simulations and forecasts with the ECMWF IFS is given, for example, by  $T_L159L91$ , indicating a truncature retaining 159 spectral coefficients for the dynamics, a linear grid for the physics with 160 latitudes and up to 320 longitudes, and 91 levels in the vertical direction.

### a. A climatology of land surface albedo derived from MODIS observations

A new climatology of land surface albedo has been introduced in the IFS to be used as boundary conditions in shortwave flux computations. Apart from being derived from more recent and more spatially detailed satellite observations than the previously operational land surface albedo derived from ERBE observations (Sellers et al. 1996), this MODIS albedo will be consistent with the MODIS-derived surface reflectances that will be used when computing synthetic MODIS radiances for aerosol analysis as part of the Global Earth Monitoring Using Satellite and In Situ Data–Aerosol subproject (GEMS–AER).

This new climatology was derived from the 2001–2004 datasets produced by Boston University (Schaaf et al. 2002), with processing over 16-day periods of the 1-km spatial resolution MODIS observations. The wideband albedo, given for direct and diffuse radiation in both the UV-visible and near-infrared parts of the shortwave spectrum, replaces the monthly-mean spectrally flat albedo previously derived from ERBE observations. Figure 1 presents for the month of April the UV-visible ( $0.3\text{--}0.7 \mu\text{m}$ ) and near-infrared ( $0.7\text{--}5.0 \mu\text{m}$ ) components of the shortwave albedo derived from MODIS. Figure 2 compares the previous operational

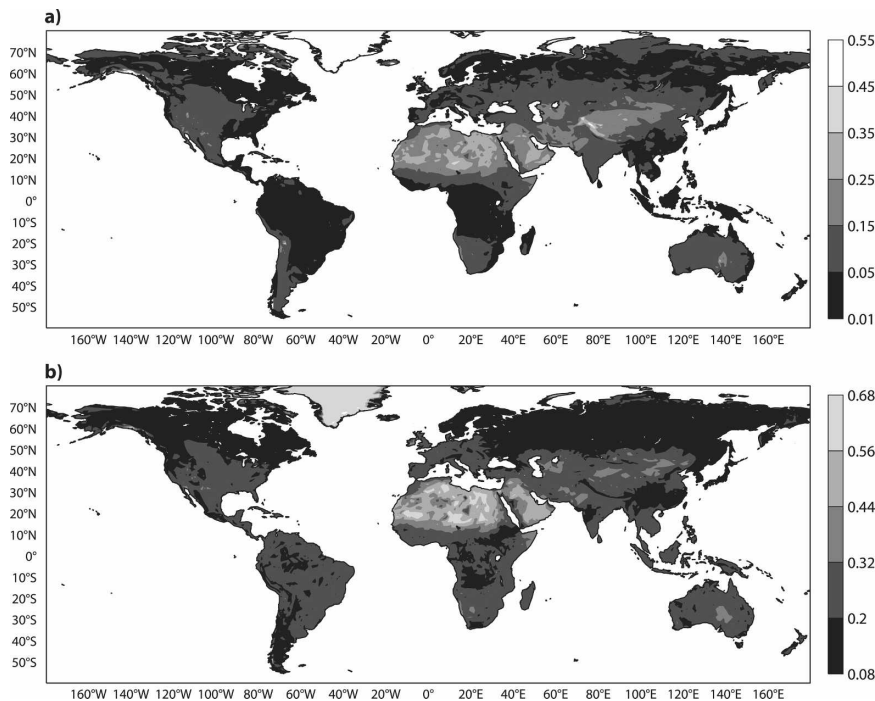


FIG. 1. The land surface albedo derived from MODIS observations for April at  $T_{L799}$ . (a) UV-visible ( $0.3\text{--}0.7\ \mu\text{m}$ ) and (b) near-infrared ( $0.7\text{--}5.0\ \mu\text{m}$ ) parts of the shortwave spectrum.

spectrally flat ( $0.3\text{--}5.0\ \mu\text{m}$ ) land surface albedo derived from ERBE observations, with the equivalent surface albedo obtained from the ratio of the upward over downward shortwave fluxes computed with the new albedo.

Sets of 13-month-long integrations at  $T_{L159L91}$  were conducted with the two different representations of land surface albedo and the two radiation configurations (preMcRad and McRad) within CY32R2 of the operational library. As seen in Table 2, the impact of the change from ERBE-derived to MODIS-derived land surface albedo on the climate of the IFS  $T_{L159L91}$  model is small, whatever the radiation configuration. With the previous radiation configuration, the change of land surface albedo was somewhat detrimental, whereas with the McICA-based radiation, the change of land surface albedo brings some small improvements to the representation of the climate. Despite what could be thought of as some sizeable changes in local albedo features (e.g., a general increase of about 0.05 over the Sahara Desert and a decrease of up to 0.10 over south of central Russia), the impact in 10-day forecasts at  $T_{L399L62}$  from the change in surface albedo is marginal. Figure 3 compares, for the model with ERBE and MODIS albedos, the parameter the most sensitive to this albedo change (mean error in temperature at 850 hPa). With the pre32R2 radiation package, the differ-

ence remains within 0.02 K after 10 days; it is slightly bigger (up to 0.08 K after 10 days in the Northern Hemisphere) with the McRad radiation package. These differences are very small and do not translate to any sizeable change in other parameters. Similar results are found for the  $T_{L799L91}$  model configuration.

#### b. What is McICA?

At the grid scale of a large-scale atmospheric model (LSAM), domain-averaged radiative fluxes in clouds with substantial horizontal and vertical variability can, in principle, be determined quite accurately using the plane-parallel independent column approximation (ICA) by averaging the flux computed for each class of cloud in turn (Cahalan et al. 1994; Barker et al. 1999). This approach neglects true three-dimensional effects, but those effects are generally minor (Barker et al. 2003). Unfortunately, this ICA-based method is too computationally expensive for dealing with radiation transfer in a LSAM. Various approximations have been introduced over the years to compute domain-averaged radiative fluxes for internally variable clouds, all invoking assumptions about the nature of the horizontal variability (e.g., Stephens 1988; Oreopoulos and Barker 1999; Cairns et al. 2000) or how cloud layers are linked over the vertical (Geleyn and Hollingsworth 1979; Morcrette and Jakob 2000; Li 2002). Regardless of what

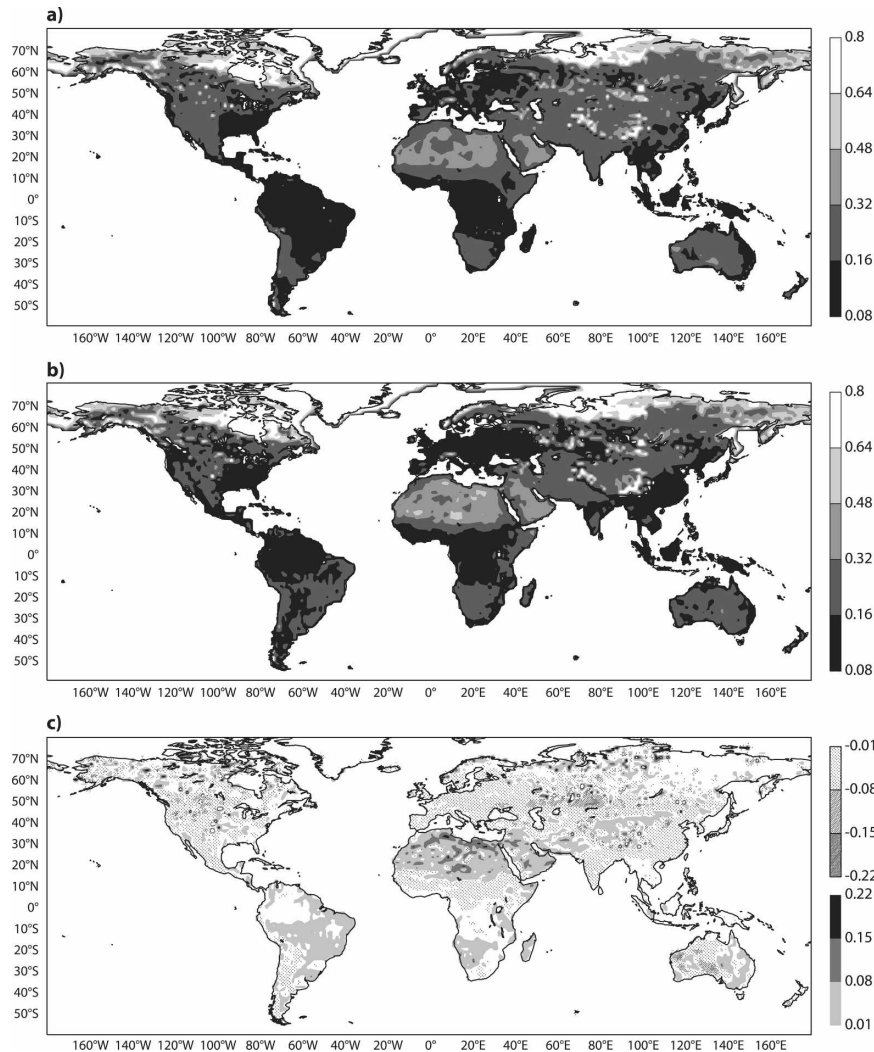


FIG. 2. The land surface albedo over the entire shortwave spectrum for April, as seen in the model at  $T_{L799}$ . (a) The spectrally flat ERBE-derived albedo, (b) the equivalent albedo obtained using the various MODIS-derived albedo components, and (c) the difference between the model with MODIS and ERBE albedos.

assumptions are made about these unresolved structures, estimates of radiative heating should theoretically become increasingly unbiased at increasingly large spatial and temporal scales. However, this is generally

not the case, and climate simulations have been shown to be very sensitive to seemingly small, but systematic, alterations to cloud optical properties (e.g., Senior 1999).

TABLE 2. Annual means from 13-month cycle OPE simulations (first month is discarded) at  $T_{L159L91}$  with the ERBE- and MODIS-derived land surface albedos. Radiative fluxes at the TOA are compared with CERES measurements: OLR, ASW, LWCF, and SWCF ( $W m^{-2}$ ) are defined in section 3a. Total precipitation (TP;  $mm day^{-1}$ ) is compared with GPCP data. For the model, bias and standard deviation (in parentheses) are given for the previously operational Rad and McRad models.

	OLR	ASW	LWCF	SWCF	TP
Observed	-239	244	27.3	-48.7	2.61
Rad ERBE	-8.1 (12.7)	-10.0 (17.5)	-9.6 (13.6)	-5.2 (15.4)	0.45 (1.39)
Rad MODIS	-8.4 (12.8)	-10.2 (17.0)	-9.8 (13.8)	-5.3 (15.1)	0.42 (1.30)
McRad ERBE	-3.4 (8.3)	-6.3 (14.7)	-4.2 (8.2)	-0.0 (13.1)	0.42 (1.30)
McRad MODIS	-3.2 (7.9)	-5.8 (14.2)	-4.0 (7.9)	-0.2 (12.9)	0.40 (1.21)

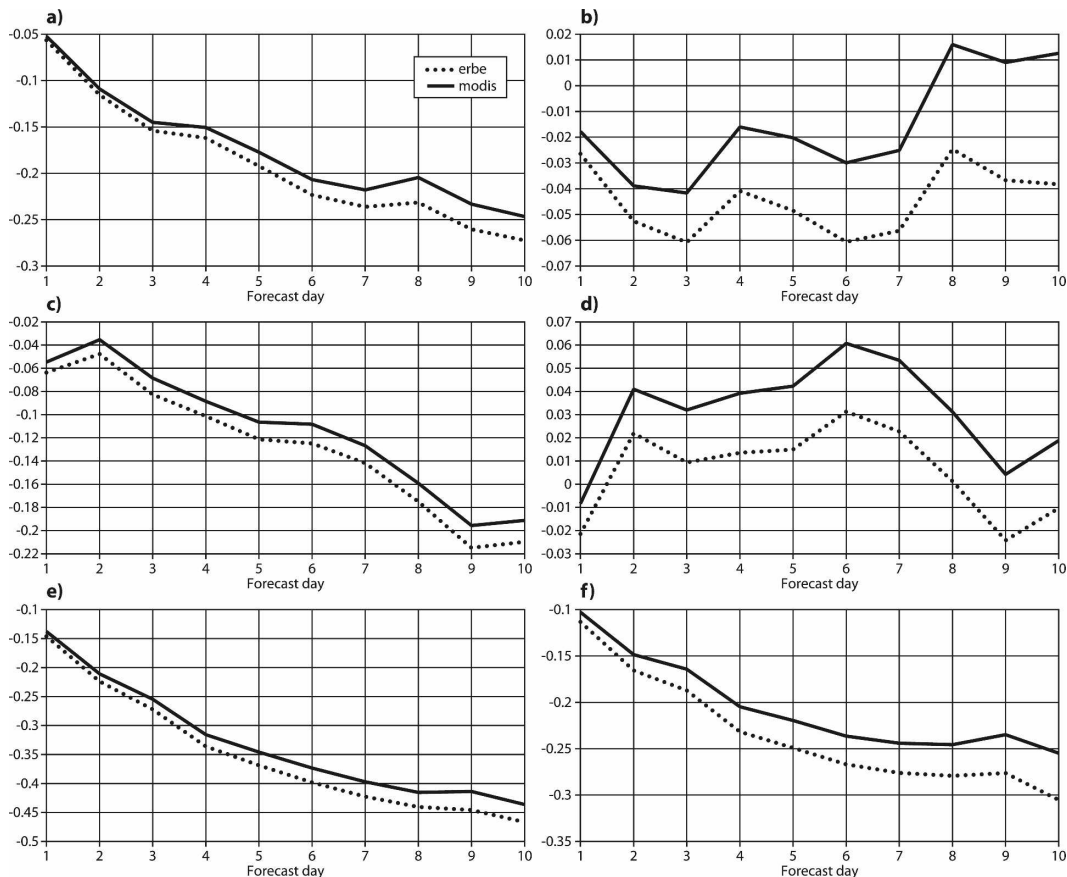


FIG. 3. The mean error of the temperature at 850 hPa for the (a), (b) Northern Hemisphere, (c), (d) tropics, and (e), (f) Southern Hemisphere from sets of 93 10-day forecasts at  $T_1399L62$ , started every 96 h from 1200 UTC 2 February 2006 to 1200 UTC 5 February 2007 with the CY32R2 of the ECMWF model. (left) The pre32R2 (preMcRad) radiation configuration and (right) the 32R2 McRad configuration; solid and dashed curves correspond to the MODIS- and ERBE-derived land surface albedos, respectively.

Recently, Barker et al. (2002) and Pincus et al. (2003) introduced a new method for computing broadband radiative fluxes in LSAMs, yielding unbiased radiative fluxes over an ensemble average of one-dimensional RT simulations. It is referred to as the McICA. The most attractive features of McICA are twofold: first, it extricates the description of the subgrid-scale cloud structure from the radiative transfer algorithm through a cloud generator that provides the cloud parameters for the radiation schemes by sampling the cloud information randomly from the cloud fraction and water profiles provided by the LSAM; second, its radiative fluxes, unbiased with respect to ICA, are consistent with assumptions made about the unresolved structure in other parts of the model [e.g., the overlap assumption implicit in the calculations of precipitation from cloud layers and evaporation in the noncloudy parts of underlying layers (Jakob and Klein 1999)]. In practice, this subgrid-scale cloud structure is related either to the

overlapping of the cloud layers in the vertical and/or to the horizontal variability of the cloud characteristics. Whether in the vertical or in the horizontal, the cloud characteristics referred to above correspond to input parameters in a traditional radiation transfer scheme, namely, the distribution of condensed water in various phases, that of the particle effective dimension, which together with the distribution of intervening gases should define the radiation exchange on the vertical within a grid of the LSAM. ICA and McICA do not account for true three-dimensional transfer effects, but those effects can generally be neglected as shown by Räisänen et al. (2003) using fields produced every 3 h over a day by a cloud-resolving model (CRM) embedded in a LSAM.

The McICA approach is an approximation to the full ICA. As discussed by Barker et al. (2002) and Pincus et al. (2003), for the full ICA, the average monochromatic radiative flux, over a domain that has been subdivided

TABLE 3. Characteristics of the longwave and shortwave radiation schemes in McRad.

	RRTM <sub>LW</sub>	RRTM <sub>SW</sub>
Solution of RT equation	two-stream method	two-stream method
Number of spectral intervals	16 (140 g points)	14 (112 g points)
Absorbers	H <sub>2</sub> O, CO <sub>2</sub> , O <sub>3</sub> , CH <sub>4</sub> , N <sub>2</sub> O, CFC11, CFC12, aerosols	H <sub>2</sub> O, CO <sub>2</sub> , O <sub>3</sub> , CH <sub>4</sub> , N <sub>2</sub> O, CFC11, CFC12, aerosols
Spectroscopic database	HITRAN-96	HITRAN-96
Absorption coefficients	from LBLRTM	from LBLRTM
Cloud handling	true cloud fraction	true cloud fraction
Cloud overlap assumption as set up in cloud generator	maximum-random* generalized**	maximum-random* generalized**
	Cloud optical properties	
Method	16-band spectral emissivity from $\tau$ , $g$ , $\omega$	14-band $\tau$ , $g$ , $\omega$
Ice clouds data	Ebert and Curry (1992)* Fu et al. (1998)**	Ebert and Curry (1992)* Fu (1996)**
Water clouds data	Smith and Shi (1992)* Lindner and Li (2000)**	Fouquart (1987)* Slingo (1989)**
Effective liquid droplet size	Martin et al. (1994)	Martin et al. (1994)
Effective ice particle size	Sun (2001)	Sun (2001)
Reference	Mlawer et al. (1997) Morcrette et al. (2001)	Clough et al. (2005)

\* Configuration operational up to CY31R2.

\*\* Configuration operational with McRad.

into  $N$  columns in which each layer can only have a cloud fraction of 0 or 1, is

$$\langle F \rangle = \frac{1}{N} \sum_{n=1}^N F_n. \quad (1)$$

In subcolumn  $n$ , using a radiation parameterization (plane parallel and considering a homogeneous cloud water distribution in all overcast layers) with a correlated- $k$  distribution (CKD) approach (Lacis and Oinas 1991) to deal with absorption, the total flux  $F_n$  is

$$F_n = \sum_{k=1}^K c_k F_{n,k}, \quad (2)$$

where the summation is over the  $K$  absorption coefficients, and  $c_k$  is the corresponding width of the part of the spectrum corresponding to the absorption coefficient  $k$  (spectral subinterval  $k$ ) in the correlated- $k$  distribution.

Combining (1) and (2) gives

$$\langle F \rangle = \frac{1}{N} \sum_{n=1}^N \sum_{k=1}^K c_k F_{n,k}. \quad (3)$$

A radiation code that explicitly integrates the double sum in (3) would be far too expensive for GCM applications. The McICA solution to this problem is to approximate (3) as

$$\langle F \rangle_M = \sum_{k=1}^K c_k F_{n_k,k}, \quad (4)$$

where  $F_{n_k,k}$  is the monochromatic radiative flux in spectral subinterval  $k$ , with a randomly selected vertical cloud distribution  $n_k$ . From this definition, the McICA solution (4) is equal to the ICA solution only when all  $N$  subcolumns are identical or when  $N = 1$ . As discussed in Räisänen and Barker (2004), McICA's incomplete pairing of subcolumns and spectral intervals ensures that its solution will contain random, but unbiased, errors.

McICA can in principle be used within any radiation transfer scheme provided the following conditions: 1) a cloud generator is used to define how the cloud information is distributed over each spectral element in the radiation spectrum, and 2) enough  $g$  points (or spectral intervals) are available to make the profiles of cloud fraction and cloud water resulting from the summation over the whole distribution consistent with the original profiles. The application of the McICA approach involves using a cloud generator together with slightly modified but otherwise standard radiation schemes. A description of the radiation transfer schemes and of the cloud generator used in this study is given below.

### c. Practical implementation of McICA in the ECMWF model

Table 3 summarizes the main features of the radiation package used in the operational model since 5 June

2007. The radiation fluxes are computed using the RRTM, both in the longwave and shortwave parts of the spectrum.

The ECMWF version of  $\text{RRTM}_{\text{LW}}$  (Mlawer et al. 1997; Morcrette et al. 2001) describes the longwave spectrum, with 16 spectral intervals corresponding to a total of 140  $g$  points [ $K_{\text{LW}} = 140$  in Eq. (4)].  $\text{RRTM}_{\text{SW}}$  (Clough et al. 2005) describes the shortwave spectrum, with 14 spectral intervals corresponding to a total of 112  $g$  points [ $K_{\text{SW}} = 112$  in Eq. (4)]. Each of the 16/14 spectral intervals might have a different number of  $g$  points (in the cumulative probability space directly derived from the correlated- $k$  distribution), depending on by how much the absorption coefficient varies within the spectral interval but also how much the spectral interval contributes overall to the total flux, and this over the whole depth of the atmosphere represented by the atmospheric model.

For each of these  $g$  points, an essentially monochromatic-type radiation transfer is carried out using a two-stream method with an approximation of LW scattering and using a Delta two-stream method with SW scattering. For liquid water clouds, the effective droplet radius is diagnosed from the cloud liquid water content following the method of Martin et al. (1994); the effective ice particle size is diagnosed from the cloud ice water content following a modification of Ou and Liou (1995) in the reference scheme and following the method of Sun (2001) in the McRad scheme.

The McICA versions of  $\text{RRTM}_{\text{LW}}$  and  $\text{RRTM}_{\text{SW}}$  differ from the above versions in two respects. First, avoiding any explicit reference to cloud fraction greatly simplifies the parts of the algorithms devoted to the vertical integration, which now deal simply with optical thicknesses. For a given  $g$  point, a cloud, when present fully, occupies a model layer. Therefore, cloudy calculations only involve modifying the optical parameters (optical thickness  $\tau$ , single scattering albedo  $\omega$ , and asymmetry factor  $g$ ). Second, this allows for the removal of the 0.7 factor multiplying the cloud optical thickness, which had been introduced in 1997 (Cahalan et al. 1994; Tiedtke 1996) in the ECMWF IFS to approximately account for the effect of cloud inhomogeneities at the subgrid level.

As stated in section 2b, the McICA representation of cloud-radiation interactions requires the cloud information to be distributed by a cloud generator over the vertical, with the constraint that the total cloudiness and cloud water loading for a grid point is strictly conserved for an infinite number of draws of the cloud generator (and conserved to a high degree of approximation for a large number of draws, as with 140 in the LW and 112 in the SW).

The purpose of the cloud generator is, starting from a cloud profile (cloud fraction and cloud water content) provided by a traditional cloud scheme (e.g., Tiedtke 1993), to randomly distribute the cloud information [in terms of presence (1) or absence (0)] into each of the layers covered by the original cloud profile. This distribution is done  $N$  times (McICA with  $N$  going to infinity would be equal to ICA), with the constraint that a summation over the  $N$  profiles would recreate the original vertical distribution of partial cloudiness. In the ECMWF model, for each radiation time step (every 1 h of model time for the  $T_L799L91$  forecast) and each radiation grid point, the cloud generator is used twice to produce two cloud distributions relevant, respectively, to the 140  $g$  points of the LW and to the 112  $g$  points of the SW radiation schemes. We use the cloud generator of Räisänen et al. (2004), which can vertically distribute either the cloud cover according to a maximum-random overlap assumption (Morcrette and Jakob 2000) or both the cloud cover and cloud water, assuming a generalized overlap (Hogan and Illingworth 2000, 2003).

When present, clouds occupy the full horizontal extent of the layer, and the vertical distribution of these clouds (0 or 1 cloud cover) is defined independently for each of the 140 (112)  $g$  points of the longwave (shortwave) scheme by the cloud generator, with the constraint that the total cloudiness and cloud water loading for a grid point is conserved when  $N$  tends to infinity.

Most of the McRad results presented hereinafter correspond to a generalized overlap with decorrelation lengths of 2 km for cloud cover, 1 km for cloud water, and a standard deviation of the cloud condensate, normalized by the mean cloud condensate ( $\sigma_{\tau}/\bar{\tau}$ ) of 1. Only in section 3d will results be discussed corresponding to a generalized overlap with different decorrelation lengths or to maximum random overlap of the cloud layers. In all comparisons discussed hereinafter, the preMcRad model (CY31R2 operational model, hereinafter OPE) uses the ECMWF six-spectral-interval version of the shortwave radiation code of Fouquart and Bonnel (1980), with a slightly different set of cloud optical properties marked by a cross (+) in Table 3. In tests not discussed here, it was shown that replacing the operational shortwave radiation scheme by  $\text{RRTM}_{\text{SW}}$  alone or changing the cloud optical properties, while affecting the radiation fields, did not greatly affect the systematic errors shown by the ECMWF IFS in 13-month simulations at  $T_L159L91$ . Only the full McRad package with the suppression of the 0.7 inhomogeneity factor, the use of the McICA approach within  $\text{RRTM}_{\text{LW}}$  and  $\text{RRTM}_{\text{SW}}$ , and the revised cloud optical properties shows the positive impact discussed below.

#### d. A different radiation grid for McRad

Following a study of the dependence of radiation fields and model climate on (temporal and) spatial characteristics of the radiative forcing (Morcrette 2000), a new interface for radiation computations was developed and implemented in October 2003. Radiation calculations are performed on a grid with a coarser resolution than the current model grid. Interpolation between model and radiation grids is performed using interfaces existing within the IFS libraries and this, as a result, helps reduce code maintenance. This radiation grid had been used since October 2003, with a coarsening factor of two in both latitude and longitude w.r.t. the rest of the model (e.g., the operational forecast model at  $T_L799$  is run with a radiation grid R399).

The introduction of McRad in the ECMWF IFS brought a sizeable increase in the computer time required for carrying out a given forecast. It must be stressed that this increase is *not* related to the McICA approach, as the McICA versions of RRTM<sub>LW</sub> and RRTM<sub>SW</sub> are slightly faster than the original versions because they are not dealing with fractional cloudiness but only with optical thicknesses, whether originating from clear-sky absorbers and aerosols, or the same plus cloud optical thickness. The increase is mainly linked to the use of RRTM<sub>SW</sub>, with its 112 *g* point radiative transfer computations compared with computations over the six spectral intervals of the previously operational SW scheme (Fouquart and Bonnel 1980; Morcrette 2002a).

The implementation of the more computer-intensive McRad has therefore led to the search for an optimal radiation grid for the different weather forecasting applications run at ECMWF. Table 4 presents for the various model configurations used at ECMWF an overview of the timing with and without McRad. Depending on the model resolution, the associated time step, and the frequency for calling the full radiation schemes, the cost of the model integration increased from 15% to 29%. However, comparisons of results with the different radiation grids [from R399 to R95 for the  $T_L799L91$  high-resolution model, from R255 to R31 for the  $T_L399L62$  model run in the Ensemble Prediction System (EPS), and from R159 to R31 for the  $T_L159L91$  model used for seasonal forecasts] were systematically carried out.

For the choice of the radiation grid, a compromise has to be made between the computer time required to run a given configuration and how detailed to make the representation of the spatial cloud structure and its associated radiative fluxes. Different meteorological applications lead to different answers. For the high-resolution deterministic forecast in which the position

TABLE 4. Impact of the McRad radiation package on the timing of the ECMWF model forecasts for different configurations and horizontal resolutions, with the resolution for the dynamics (Dyn), the resolution for radiation (Rad), the frequency (hour) for calling the full radiation scheme (Freq), the fraction of computer time taken by the radiative transfer calculations (%Rad), and the factor by which McRad increases the computer cost relative to the previous OPE (Ratio).

Configuration	Dyn	Rad	Freq	%Rad	Ratio
<i>T<sub>L</sub>799L91</i>					
OPE	799	399	1	7.3	1.000
McRad	799	511	1	36.4	1.456
	799	399	1	26.5	1.262
	799	319*	1	19.2	1.147
	799	255	1	13.8	1.076
	799	159	1	6.7	0.994
	799	95	1	3.4	0.960
<i>T<sub>L</sub>399L62</i>					
OPE	399	159	3	4.1	1.000
McRad	399	255	3	31.6	1.403
	399	159	3	16.4	1.148
	399	95*	3	7.7	1.039
	399	63	3	3.8	0.998
	399	47	3	3.0	0.989
	399	31	3	2.1	0.980
<i>T<sub>L</sub>159L91</i>					
OPE	159	63	3	8.0	1.000
McRad	159	159	3	67.5	2.831
	159	95	3	45.1	1.675
	159	63*	3	27.7	1.273
	159	47	3	19.5	1.143
	159	31	3	11.0	1.034

\* Operational configuration implemented on 5 Jun 2007.

of clouds affected by land–sea temperature and orographic effects is an important information, the highest radiation resolution is to be kept as much as possible. However, it must be kept in mind that McICA allows subgrid-scale information on the horizontal distribution of cloud elements to be taken into account (via the normalized standard deviation), so what appears as a reduced radiation grid in fact includes more information than the original radiation grid used with the preMcRad scheme. For the EPS, the constraint to have the highest radiation resolution possible can certainly be released (see section 4b). A best compromise was chosen (R319 for  $T_L799$ , R95 for  $T_L399$ , and R63 for  $T_L159$ ), which allows the maximum benefit of McRad within the time constraints for delivering the various operational products. The coarsening of the radiation grid was shown to have very little impact on the objective scores provided by higher-resolution models, which are discussed in section 4.

### 3. Results for seasonal simulations at $T_L159L91$

Two sets of annual simulations with either McRad or the operational radiation package have been carried

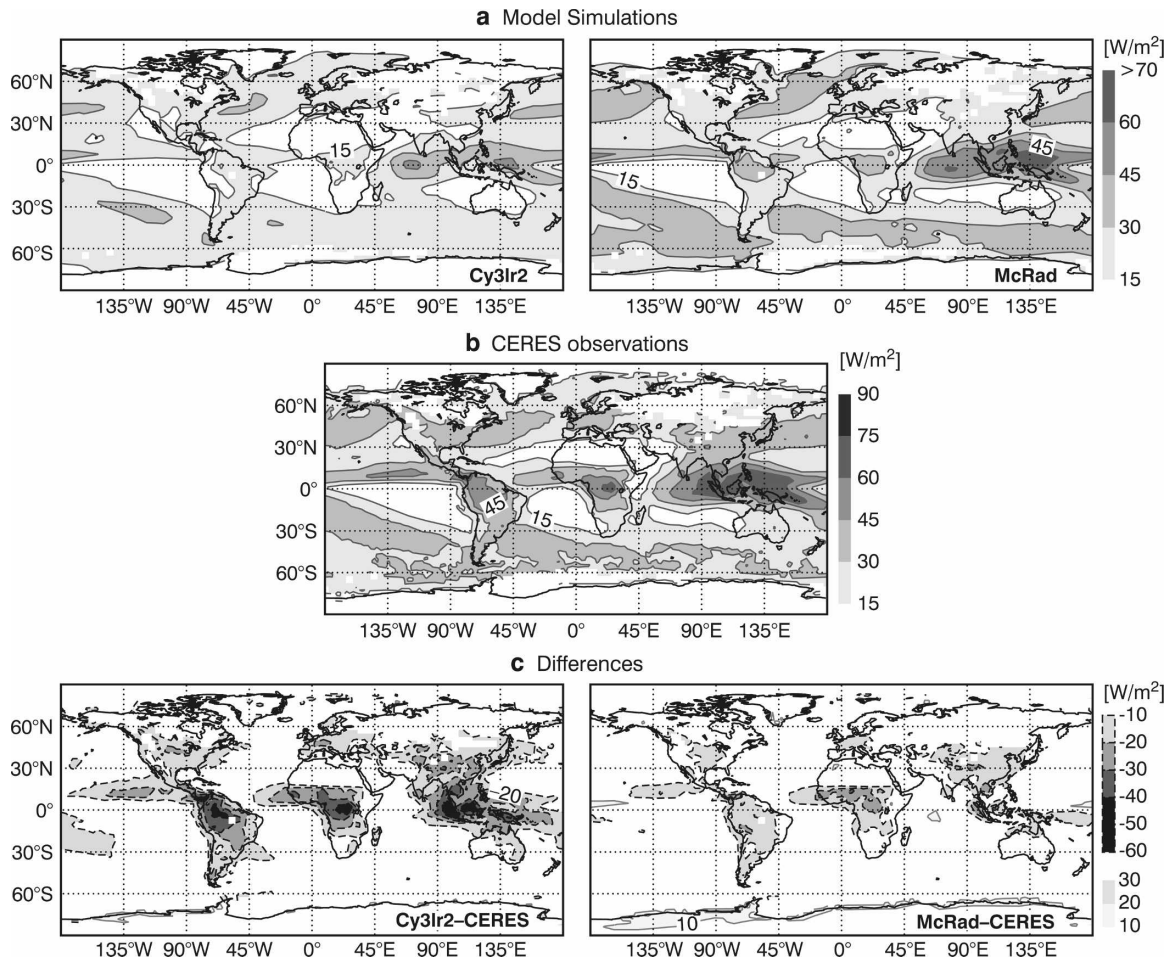


FIG. 4. Annual average of longwave cloud forcing ( $\text{W m}^{-2}$ ). (a) The ECMWF model simulations, with (left) OPE and (right) McRad; (b) the CERES observations; and (c) the differences between simulations and observations. For the model, results are for averages over three simulations starting 24 h apart, with output parameters averaged over the period September 2000–August 2001.

out over the 13-month period between August 2000 and September 2001. Each set includes an ensemble of three simulations, starting from analyzed initial conditions 24 h apart. Output parameters averaged over each ensemble and the September 2000–August 2001 period are presented as maps in Figs. 4–8. Global mean values for an extended list of parameters are given in Table 5, averaged over the year and over the December–February (DJF) and June–August (JJA) three-month periods.

#### a. Radiative fields at the top of the atmosphere

McRad improves the behavior of the model in a number of aspects: a change in the balance between longwave and shortwave radiation heating leads to a noticeable shift in the location of the tropical cloudiness. This shift is particularly striking when comparing the model longwave cloud forcing (LWCF; Fig. 4) and

shortwave cloud forcing (SWCF; Fig. 5) with corresponding parameters from Clouds and the Earth's Radiant Energy System (CERES) observations. This is mainly a feature of McICA because preliminary tests using  $\text{RRTM}_{\text{SW}}$  (without the McICA approach) instead of the operational shortwave radiation code, or with a different set of cloud optical properties, changed somewhat the overall radiation budget at the top of the atmosphere (TOA) but without affecting the negative bias linked to a too-small cloudiness over South America, Africa, and the tropical west Pacific Ocean. McRad markedly improves the TOA radiation biases over these areas. As seen in Table 5, the differences with CERES observations are improved with the new model, with a reduction of the global annual mean bias from  $-8.1$  to  $-3.2 \text{ W m}^{-2}$  for outgoing longwave radiation (OLR), from  $-10.0$  to  $-5.8 \text{ W m}^{-2}$  for the absorption of shortwave radiation (ASW), from  $-9.6$  to

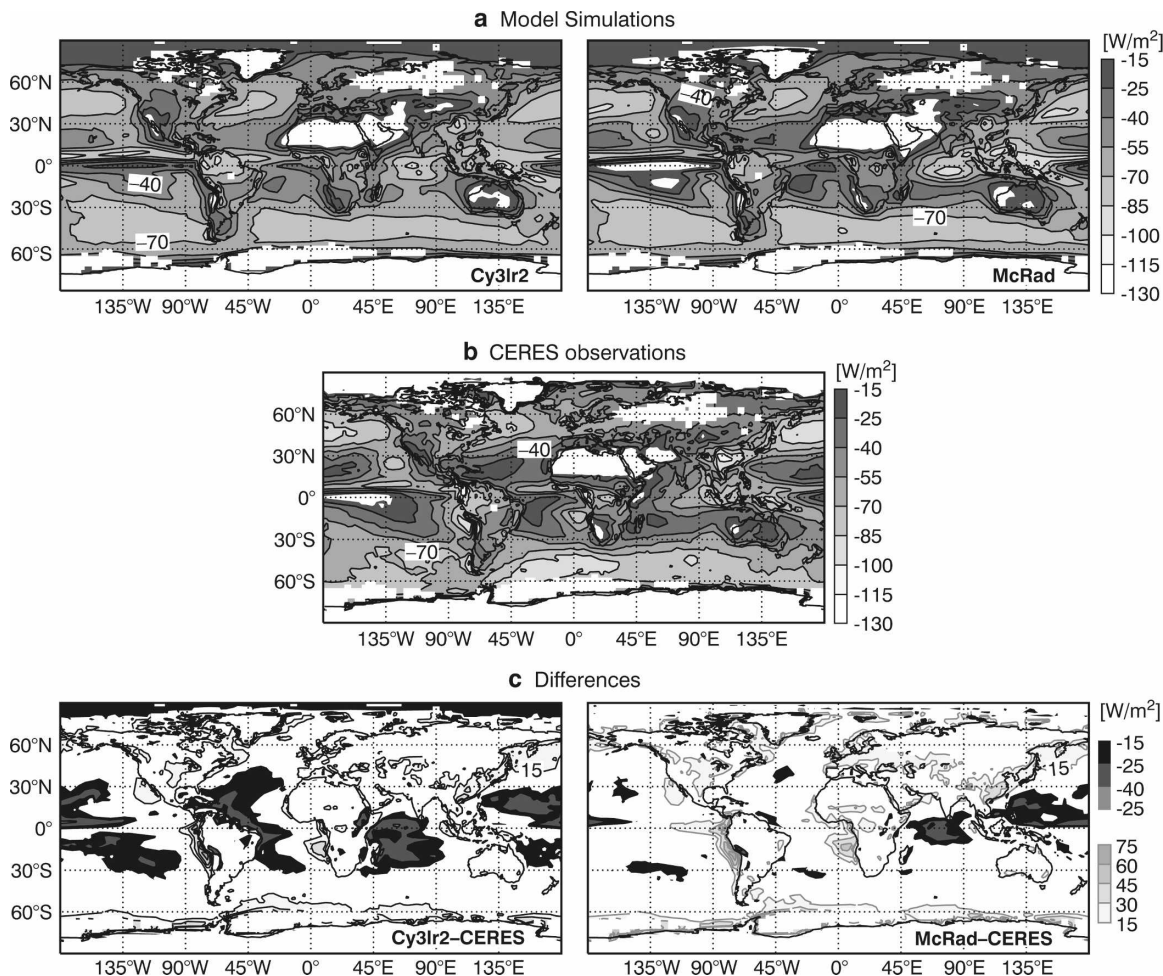


FIG. 5. As in Fig. 4, but for SWCF ( $W m^{-2}$ ).

$-4.0 W m^{-2}$  for LWCF, and from  $-5.2$  to  $-0.2 W m^{-2}$  for SWCF. More important, the reduction in biases is accompanied by the reduction in standard deviations, showing that the location of the minima and maxima of the various fields are temporally (based on monthly averages) and spatially improved by McRad. Table 4 confirms that these improvements happen over the whole year, with a general improvement on the TOA radiative parameters also appearing for DJF and JJA conditions.

From Table 5 and the related figures show that the overall climate of the model is improved in terms of the TOA radiation budget.

With McRad, the surface SW radiation is increased, which is in worse agreement with the Da Silva climatology (Da Silva and Levitus 1994; over oceans only). However, for the ECMWF model run with an interactive ocean, the better geographical distribution of SW surface fluxes produced by the new radiation package has been found to be beneficial to the forecasts of

ocean surface temperature (see section 3e). A significant improvement is also seen in temperature and humidity, when compared to the 40-yr European Centre for Medium-Range Weather Forecasts Reanalysis (ERA-40; Uppala et al. 2005).

*b. Hydrological budget*

Table 5 and the related figures show that the overall climate of the model is also improved in the global water vapor [total column water vapor (TCWV)] and cloud water distribution ([total column liquid water (TCLW)] and the level of total precipitation [(TP); compared in Table 5 with Global Precipitation Climatology Project (GPCP) and Special Sensor Microwave Imager (SSM/I) estimates]. The only degradation is seen in surface SW radiation, which shows the annual mean difference to the Da Silva–Levitus climatology (over oceans only) to be roughly doubled. This is partly linked to slightly more transparent clouds induced by the McICA approach but mostly linked to the transfer

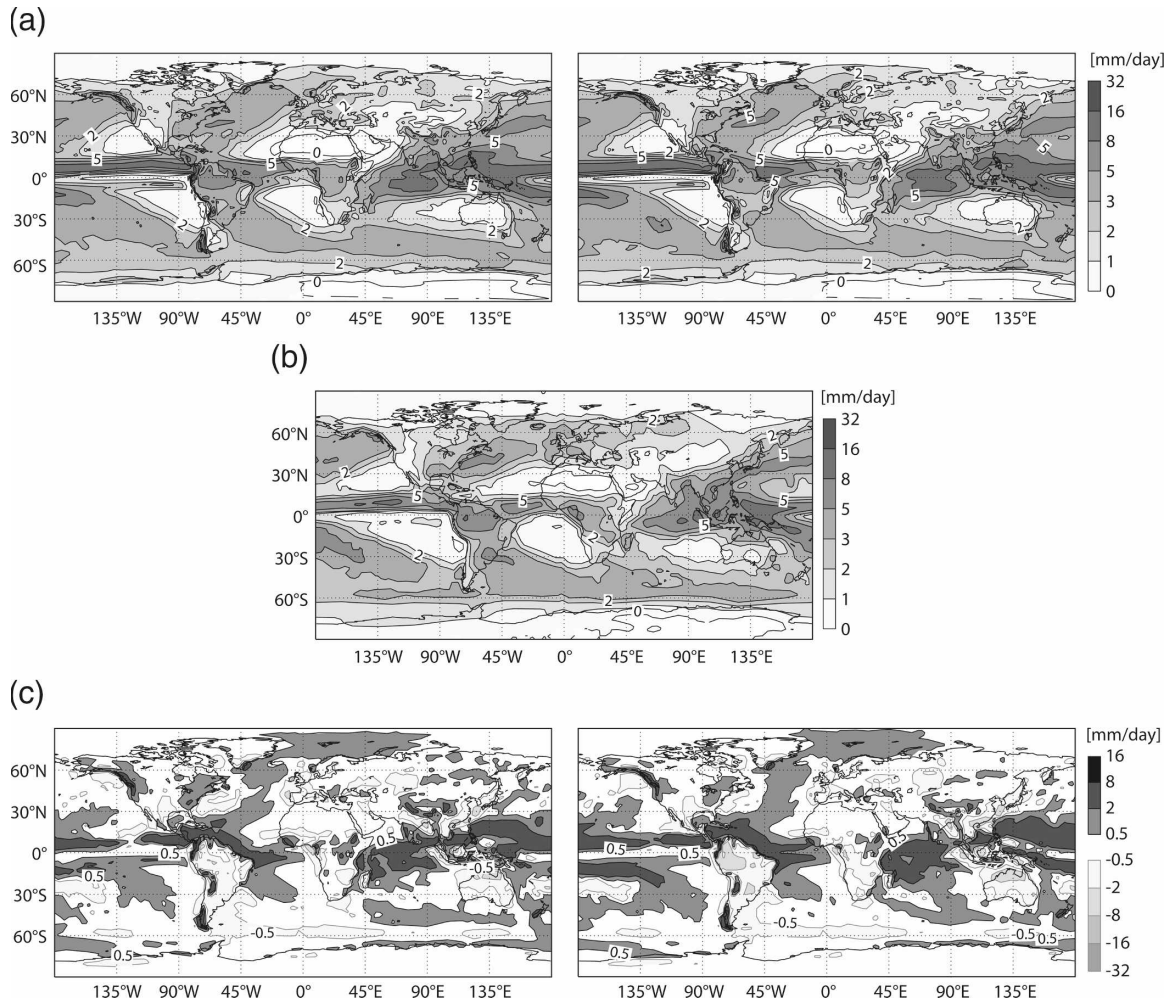


FIG. 6. As in Fig. 4, but for TP ( $\text{mm day}^{-1}$ ). (a) The ECMWF model simulations: (left) operational, and (right) McRad; (b) the GPCP observations; and (c) the differences between simulations and observations: (left) McRad, and (right) operational.

of convective cloudiness from tropical oceanic to tropical continental areas.

Despite the increase in surface SW radiation over the tropical oceans, it was found that for the ECMWF model including an interactive ocean, the better geographical distribution of surface fluxes linked to the shift of the convection produced by McRad is beneficial to the forecasts of ocean surface temperature (see section 3e).

Figure 6 presents the total precipitation and its comparison with GPCP observations. The improvements are less marked than for radiation fields. However, a reduction of the deficit of precipitation over South America and Africa and a slight reduction of the overestimation of precipitation over the Pacific, Atlantic and Indian Oceans are present. This is confirmed by the better global results on an annual or seasonal basis, seen for total precipitation in Table 5, whether com-

pared globally with GPCP or over the tropical ocean with SSM/I.

### c. Temperature, humidity, and wind errors

Figures 7 and 8 present the zonal mean differences of temperature and humidity (Fig. 7) and zonal wind and vertical velocity (Fig. 8), averaged over the year. The McRad package improves on the temperature differences (Fig. 7, top) to ERA-40 analyses, showing an overall warming of the troposphere and a cooling of the stratosphere. This translates into a slight improvement in the zonal mean humidity w.r.t. ERA-40 (Fig. 7, bottom). The impact on zonal mean zonal wind (Fig. 8, top) is somewhat smaller but generally positive. The impact on vertical velocity (Fig. 8, bottom) is mainly seen in the tropical area, with a slight decrease in both the negative and positive difference to ERA-40 between  $30^{\circ}\text{N}$  and  $30^{\circ}\text{S}$ . The differences to ERA-40 of the

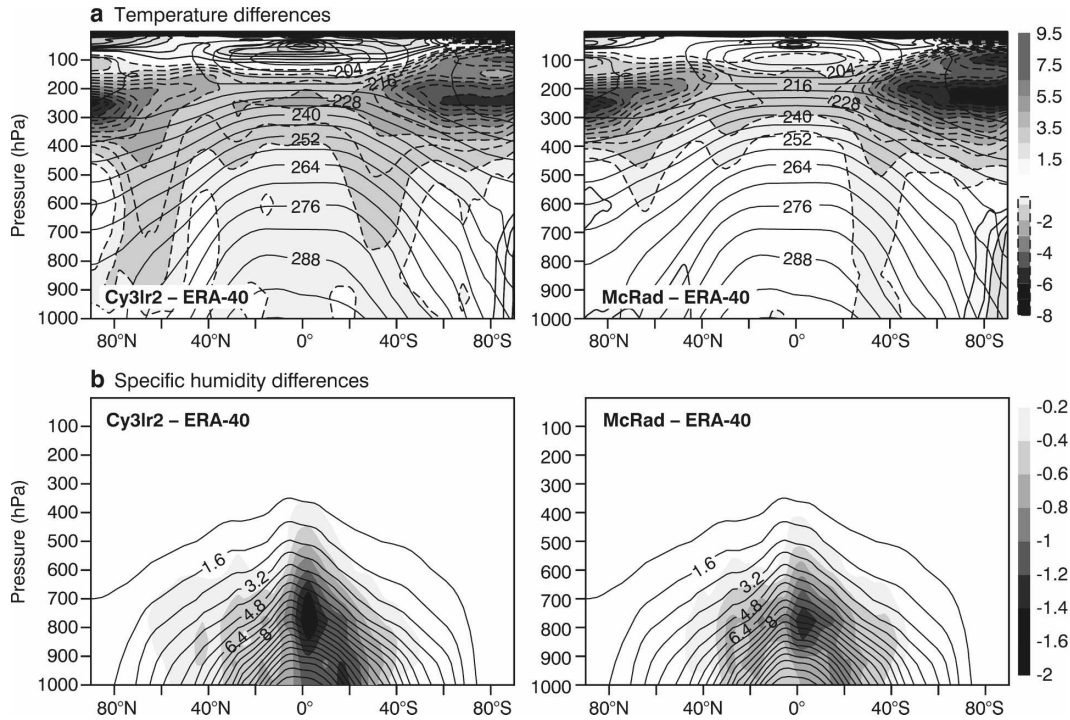


FIG. 7. Zonal mean cross section of the difference between the McRad model and the ERA-40 analysis over the 12-month period September 2000–August 2001 (shaded contours). (a) Temperature (K) and (b) humidity ( $\text{g kg}^{-1}$ ) for (left) OPE and (right) McRad. Solid lines are the ERA-40 values.

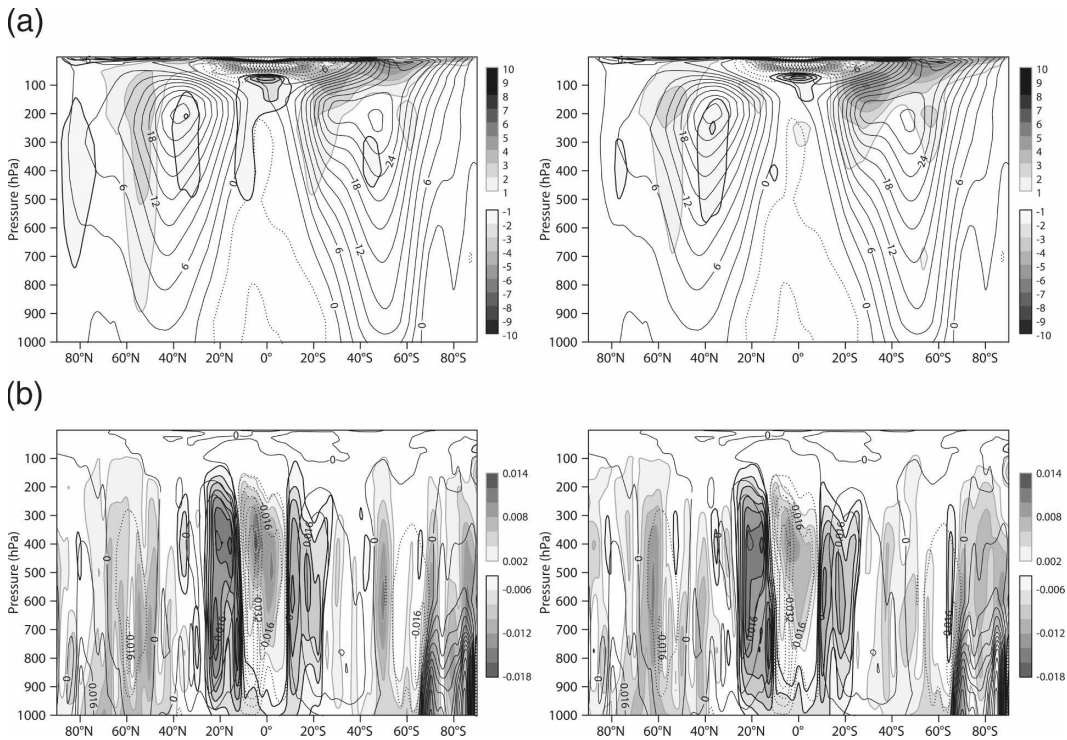


FIG. 8. As in Fig. 7, but for (a), (b) zonal wind ( $\text{m s}^{-1}$ ) and (c), (d) vertical velocity ( $\text{Pa s}^{-1}$ ) for (left) OPE and (right) McRad.

TABLE 5. Annual means from 13-month simulations at  $T_L159L91$  (first month discarded). Radiative fluxes at TOA are compared with CERES measurements, total cloud cover (TCC; %) is compared with International Satellite Cloud Climatology Project (ISCCP) D2 data, TCWV ( $\text{kg m}^{-2}$ ) and TCLW ( $\text{g m}^{-2}$ ) are compared with SSM/I data, and TP ( $\text{mm day}^{-2}$ ) is compared with GPCP or over ocean with SSM/I data. The surface fluxes over the ocean (OCN;  $\text{W m}^{-2}$ ) are compared with the Da Silva–Levitus climatology: surface net solar radiation (SSR) and solar terrestrial radiation (STR), the surface sensible heat (SSH) and latent sensible heat (SLH) fluxes, and the surface net energy flux (SNET). For the model, bias and standard deviation (in parentheses) are given for the previously operational and McRad models. At the TOA, OLR, ASW, LWCF, and SWCF are in watts per meter squared.

	Annual	DJF	JJA
OLR	-239	-236	-242
OPE	-8.1 (12.7)	-6.1 (15.0)	-5.1 (12.8)
McRad	-3.2 (7.9)	-1.1 (10.1)	-0.6 (10.5)
ASW	244	251	238
OPE	-10.0 (17.5)	-15.6 (23.9)	-9.2 (19.7)
McRad	-5.8 (14.2)	-11.4(20.5)	-5.3 (18.6)
LWCF	27.3	26.8	26.1
OPE	-9.6 (13.6)	-10.4 (16.5)	-8.3 (14.1)
McRad	-4.0 (7.9)	-4.8 (10.3)	-3.0 (9.7)
SWCF	-48.7	-52.8	-45.1
OPE	-5.2 (15.4)	-4.1 (18.6)	-6.3 (18.2)
McRad	-0.2 (12.9)	0.5 (17.0)	-1.3 (17.3)
TCC	62.2	62.9	61.4
OPE	-6.0 (10.3)	-5.7 (12.3)	-5.4 (11.8)
McRad	-5.3 (9.5)	-4.9(11.2)	-4.7 (11.4)
TP GPCP	2.61	2.58	2.63
OPE	0.45 (1.39)	0.42 (1.88)	0.43 (1.75)
McRad	0.40 (1.21)	0.37 (1.60)	0.41 (1.72)
TP SSM/I	3.80	3.57	3.66
OPE	0.67 (2.45)	0.57 (3.56)	0.44 (3.90)
McRad	0.50 (2.23)	0.38 (3.32)	0.35 (3.81)
TCWV	29.0	27.7	29.3
OPE	-2.10 (3.65)	-2.27 (4.29)	-1.73 (3.69)
McRad	-1.67 (3.13)	-1.80(3.63)	-1.25 (3.32)
TCLW	82.2	80.4	84.3
OPE	1.67 (22.1)	3.13 (33.4)	-1.11 (30.6)
McRad	0.86 (22.4)	2.05 (32.8)	-1.21 (30.8)
SSR OCN	155.2	163.7	143.7
OPE	8.4	15.1	0.3
McRad	15.6	21.9	7.4
STR OCN	-51.8	-52.5	-50.4
OPE	0.6	1.0	1.3
McRad	-0.1	0.3	0.6
SSH OCN	-11.0	-13.7	-9.0
OPE	-4.7	-3.0	-5.9
McRad	-3.5	-2.0	-4.9
SLH OCN	-96.5	-100.2	-94.2
OPE	-10.5	-7.7	-11.1
McRad	-7.2	-4.5	-7.9
SNET OCN	-2.1	-0.9	-7.9
OPE	-8.1	3.6	-17.3
McRad	2.8	14.0	-6.8

annual mean of the wind at 200, 700, and 925 hPa (Fig. 9) show that McRad has a beneficial impact at all heights, with a decrease of the errors over the tropical oceans. Particularly noticeable is the joint decrease of the mean wind error over the equatorial Indian Ocean and the central north-equatorial Pacific, both at 925 and 200 hPa; the signal over the Pacific is consistent with an improvement of the Ferrel circulation.

#### d. Sensitivity to cloud overlap assumption

As already indicated in section 2c, the use of a cloud generator external to the LW and SW radiation schemes to deal with the vertical overlap of cloud layers and the potential inhomogeneity in the horizontal distribution of cloud water content makes the testing of various configurations easy. Sets of seasonal simulations were carried out in the same conditions as those discussed in the previous sections, with the McRad model configuration and different assumptions for the cloud vertical overlap and horizontal distribution of cloud water. As can be seen in Fig. 10, the temperature impact of various decorrelation lengths for cloud cover (DLCC) or cloud water (DLCW), or switching to a maximum-random cloud overlap with provision for inhomogeneous cloud water distribution is much smaller than the impact of introducing the new radiation package. As can be seen in Table 6, each of these configurations is slightly different in terms of impact on radiation and other physical fields, and the configuration chosen for the operational implementation in CY32R2 is the one that gives the best overall comparisons to observations.

#### e. Impact on climate integrations with a coupled ocean system

As part of the testing of the McRad package, sets of simulation with the model, including a coupled ocean, were run over 10 yr, starting on 1 November 1994. One of the effects of McRad, namely, the increase in downward solar radiation at the surface, has been shown to improve the simulation of the ocean temperature, particularly during the first two years of the simulations. Figure 11 presents for these two years the difference of the ocean annual mean temperature, with ERA-40 for both versions of the model and the difference between the models.

Over most of the tropical region, the bias in SST is decreased between 0.3 and 0.9 K, with a complex pattern of improvement. For example, over the northern parts of the Pacific and Atlantic Oceans, McRad decreases the cold bias in SST and decreases the warm bias over the Pacific tropical area and the southern region.

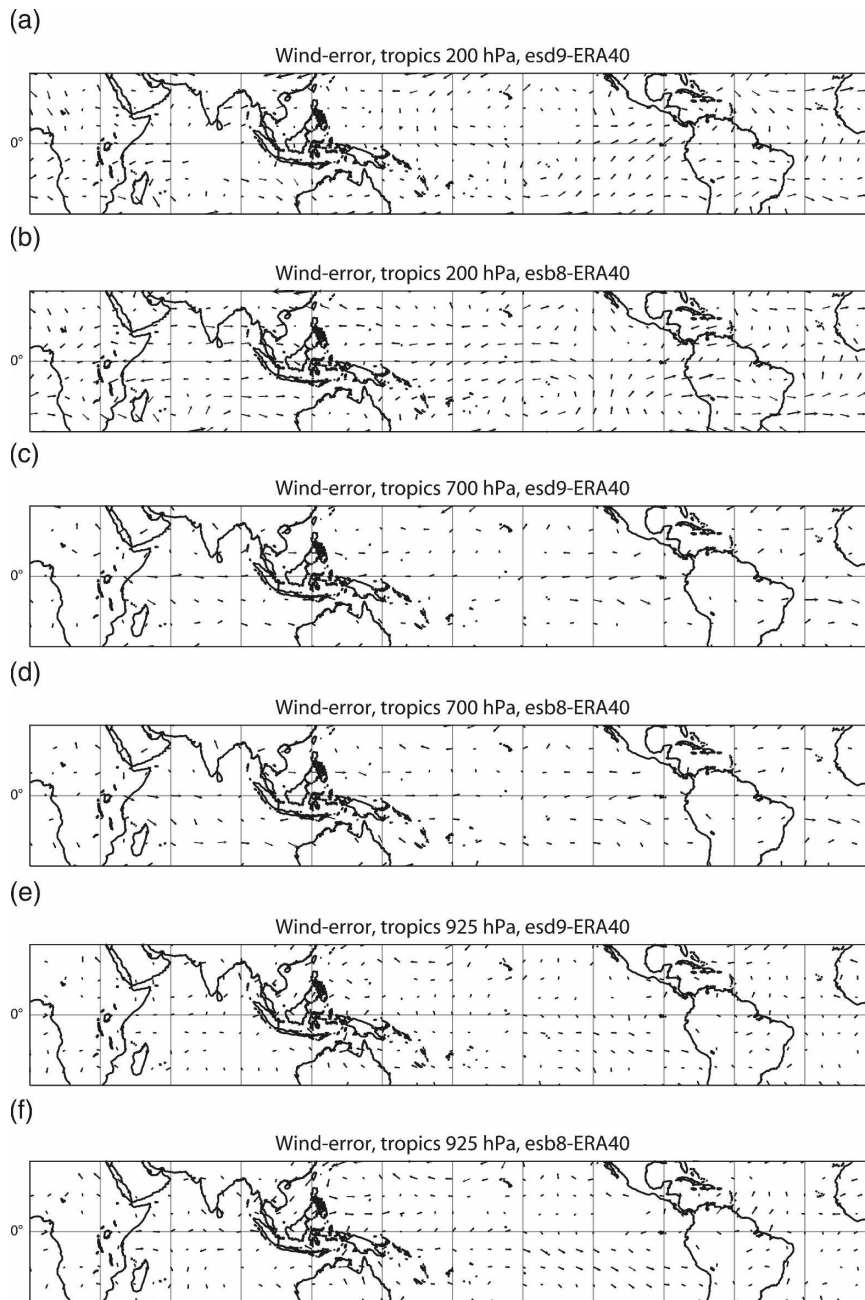


FIG. 9. The difference in wind between the annual averages from model simulations and ERA-40 for (a), (b) 200 hPa, (c), (d) 700 hPa, and (e), (f) 925 hPa. For each pair: (top) McRad and (bottom) OPE.

**4. Impact on operational weather forecasts**

*a. High-resolution deterministic 10-day forecasts at  $T_L799L91$*

An experimental suite, parallel to the operational suite at  $T_L799L91$ , was run from July 2006 to April 2007. It included McRad and a series of data assimilation modifications that were unlikely to affect the ra-

diative fluxes beyond the first few hours in the forecasts. Hereinafter, results are presented for the period December 2006–April 2007, with more specific diagnostics for January 2007. It must be stressed that the model response at  $T_L799$  is similar to what was shown in section 3 for the seasonal simulations. Here, the emphasis is put on the short-term response (12 h–10 days) of the model and on objective scores. The main impact

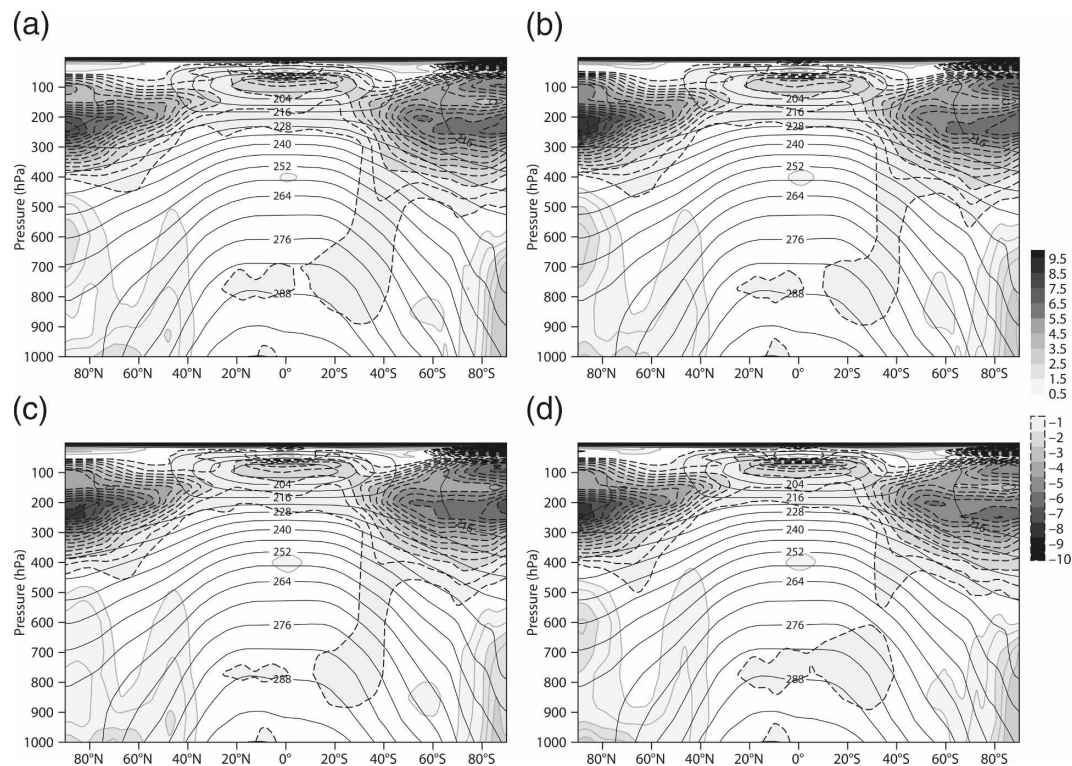


FIG. 10. The difference from ERA-40 analysis (shaded contours) for temperature (K; solid lines are the ERA-40 values) for (a) McRad model with generalized overlap of cloud layers with a DLCC = 2 km and a DLCW = 1 km, (b) DLCC = 4 km and DLCW = 2 km, (c) DLCC = 5 km and DLCW = 1 km, and (d) McRad model with maximum-random overlap of homogeneous clouds.

of McRad, relative to the previously operational radiation scheme, is to modify separately the vertical distributions of the additional longwave and shortwave heating induced by the presence of the clouds. This is

linked first to the McICA approach, which replaces the previous 0.7 inhomogeneity factor that scales all cloud optical thicknesses in the longwave and shortwave parts of the spectrum in the previous version of the radiation

TABLE 6. Results from 13-month cycle OPE simulations at  $T_L159L91$  with different cloud configurations. G21 is the McRad model with generalized overlap of cloud layers with DLCC = 2 km and DLCW = 1 km, G42 is with DLCC = 4 km and DLCW = 2 km, G51 with DLCC = 5 km and DLCW = 1 km and the McRad model with maximum-random overlap of homogeneous clouds is MR. All quantities are annual means. Radiative fluxes at TOA are compared with CERES measurements, TCC with ISCCP D2 data, and TCWV and TCLW with SSM/I data. The TP is compared with GPCP or SSM/I data (over ocean). The surface fluxes are compared with the Da Silva-Levitus climatology.

	Observation	G21	G42	G51	MR
OLR	-239	-2.7 (7.8)	-4.3 (8.1)	-3.9 (7.8)	0.02 (8.3)
ASW	244	-5.9 (14.6)	-1.8 (12.5)	-1.9 (12.3)	-13.1 (19.5)
LWCF	27.3	-2.6 (6.9)	-4.0 (7.3)	-3.6 (7.0)	0.03 (7.5)
SWCF	-48.7	-0.2 (13.4)	3.8 (12.6)	-3.7 (12.4)	-7.5 (17.2)
TCWV	29.0	-1.38 (3.06)	-1.43 (3.03)	-1.40 (3.02)	-1.18 (2.92)
TCC	62.2	-1.04 (11.1)	-1.14 (11.0)	-1.00 (10.7)	-0.12 (10.9)
TCLW	82.2	-7.44 (22.7)	-7.45 (22.8)	-7.31 (22.7)	-5.37 (22.2)
TP GPCP	2.61	0.30 (1.17)	0.31 (1.15)	0.30 (1.14)	0.29 (1.19)
TP SSM/I	3.80	0.31 (2.16)	0.30 (2.14)	0.26 (2.10)	0.31 (2.23)
SSR OCN	155.2	15.9	20.1	19.9	7.3
STR OCN	-51.8	-3.6	-5.0	-4.9	-0.5
SSH OCN	-11.0	-1.6	-1.6	-1.5	-1.5
SLH OCN	-96.5	-4.2	-4.1	-3.5	-4.1
SNET OCN	-2.1	4.5	7.4	7.9	-0.8

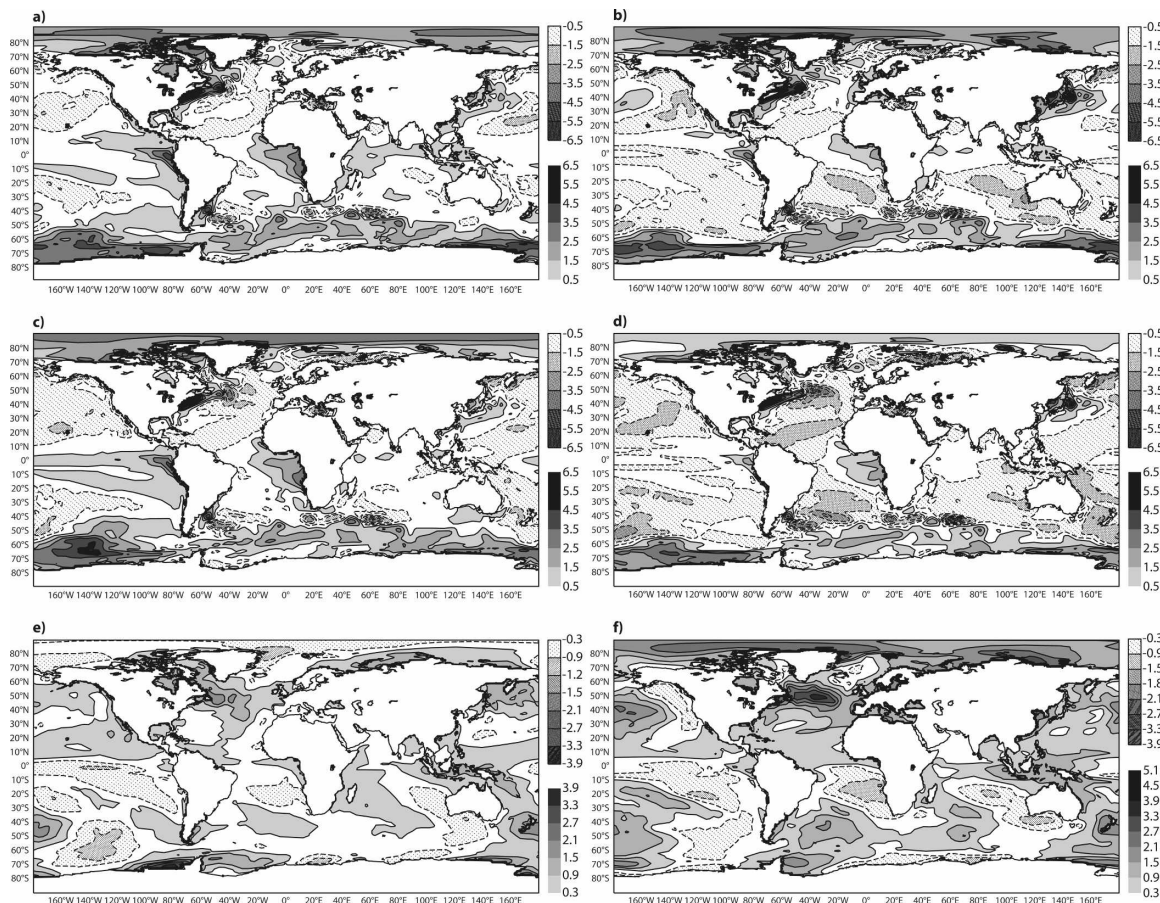


FIG. 11. Comparison of annual mean SST (K) produced by the  $T_L159R63$  model for (left) year 1 and (right) year 2. (a), (b) the differences between the McRad 32R2 model and ERA-40 SSTs, (c), (d) the differences between the OPE model and ERA-40 SSTs, (e), (f) the differences between the McRad and OPE models.

scheme, and second, to a lesser degree, is linked to the revised cloud optical properties, particularly for ice clouds in which the effective particle size is now diagnosed from temperature and the local ice water content (only temperature with the operational configuration).

For clouds with the same profiles of cloud fraction and optical thickness, the McICA approach lets more shortwave radiation reach the surface than a non-McICA scheme. In the tropics (shown in Fig. 12 as 10°N–30°S for January), this increase in downward shortwave radiation at the surface (Fig. 12a) is not compensated by an increased loss of longwave radiation as a result of a more transparent atmosphere (Fig. 12b). The resulting effect is a heating of the land surface (Fig. 12c), making the atmosphere more unstable above and increasing the convection and subsequent precipitation (Fig. 12d). This also impacts the amount of cloudiness. Over Africa, a reduction in low-level cloudiness is accompanied by an increase in low-level cloudiness eastward (Fig. 12e). Over South America, the reduction in

low-level cloudiness over the east of the Amazon basin does not translate into any clear signal. For total cloudiness (Fig. 12f), the signal is even less apparent because some vertical arrangement occurs with a reduction in the amount of low-level cloudiness, often corresponding to an increase in upper-level cloudiness.

The increase in surface solar radiation over the tropical continents is reflected in the temperature (Fig. 13a), humidity (Fig. 13b), and the amount of clouds (Fig. 13c).

Over the whole tropical belt, a slight increase in temperature is seen between about 650 and 250 hPa, and a decrease in temperature is seen at pressures below 200 hPa. Specific humidity decreases between about 650 and 250 hPa and increases between 200 and 100 hPa, with a corresponding increase in cloudiness. The impact on the zonal component of the wind (Fig. 14, left) is a weakening of the easterlies in the lower 300 hPa of the atmosphere and of the westerlies between 350 and 100 hPa. Slightly stronger ascent is seen in the vertical ve-

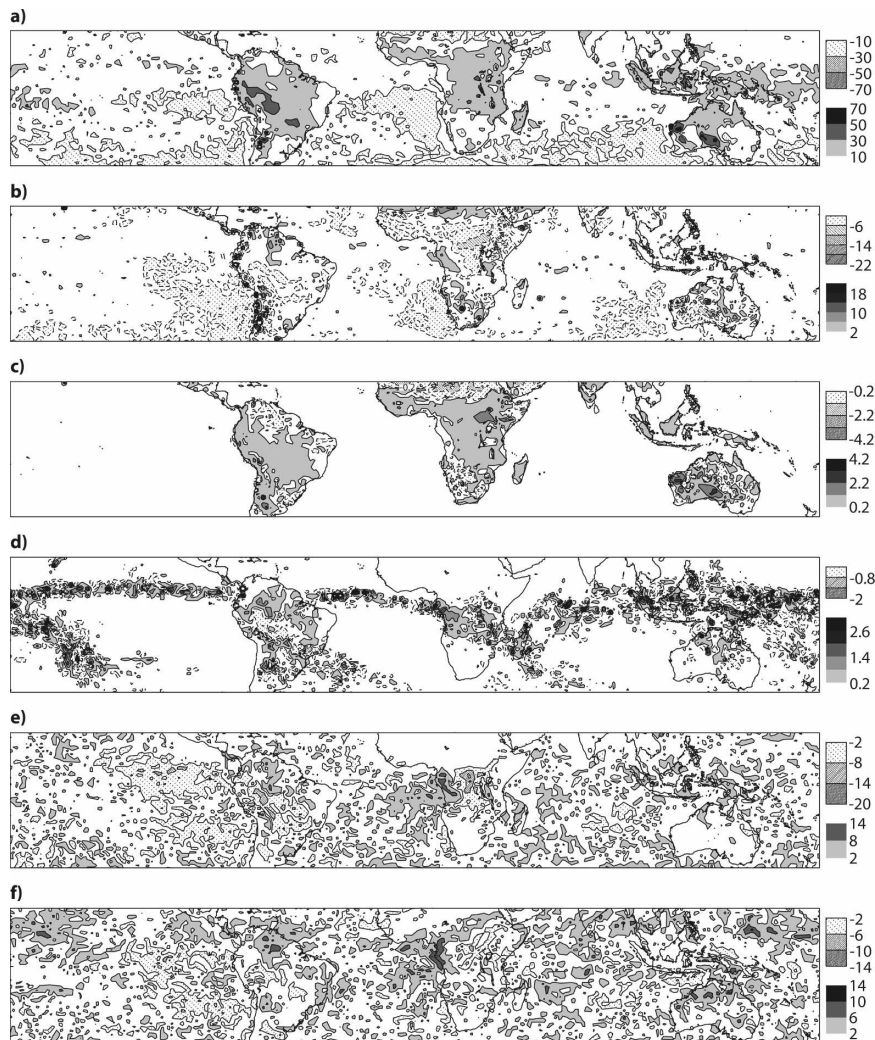


FIG. 12. Differences in surface parameters ( $\Delta x = \text{McRad} - 31\text{R2}$ ) between the McRad and the 31R2 models for January 2007. The differences in (a) net solar radiation at the surface ( $\text{W m}^{-2}$ ), (b) net longwave radiation at the surface ( $\text{W m}^{-2}$ ), (c) surface temperature (K), (d) total precipitation ( $\text{mm day}^{-1}$ ), (e) low-level cloudiness (%) and (f) total cloudiness (%). All quantities are averaged over the 62 12-h forecasts starting at 0000 UTC and 1200 UTC during January 2007.

locity (Fig. 14, right) over South America ( $70^{\circ}\text{W}$ ), Africa ( $20^{\circ}\text{E}$ ), and the tropical west Pacific ( $130^{\circ}\text{W}$ ). Given that the sea surface temperature is specified in both the long climate simulations at  $T_{L159}$  and high-resolution forecasts, the above changes are mainly driven by a change in the contrast between tropical landmasses and ocean.

In terms of radiation at the top of the atmosphere, the changes in radiative heating profiles and position of the convective activity directly affect the OLR and absorbed shortwave radiation (ASW) seen in Fig. 15, which presents the changes in OLR and ASW during the first 24 and last 24 h of the 10-day forecasts, started

every day at 1200 UTC during January 2007. In the tropical area, the decrease in OLR (a negative quantity) and the increase in ASW (a positive quantity) are consistent with more high-level cloudiness over South America, south of Africa, and the tropical west Pacific. The change over the Sahara is linked to the revised surface albedo.

The changes brought by McRad (mainly improvements in the climate simulations and a more realistic distribution of cloudiness in high-resolution forecasts from the start of the forecast) can be seen in various objective scores. Figure 16 presents the time series of the difference in rmse in geopotential at 200, 500, and

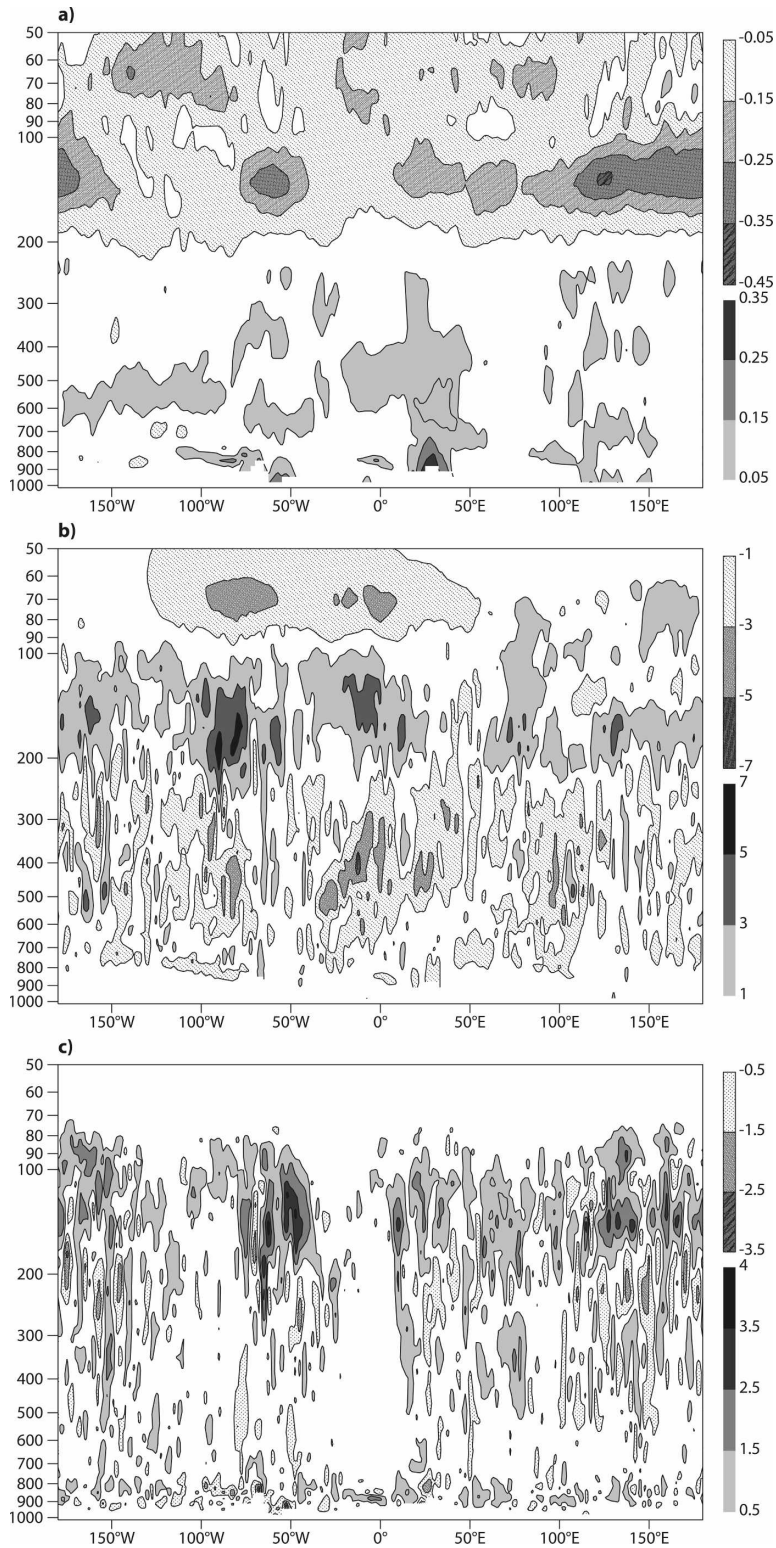


FIG. 13. As in Fig. 12, but for differences in atmospheric parameters  $\Delta x$  averaged over the 10°N–30°S latitude band. (a) Temperature ( $\Delta T$  with steps of 0.1 K from  $\pm 0.05$  K), (b) specific humidity ( $\Delta Q/Q$  with steps of 2% from  $\pm 1\%$ ), and (c) cloud cover ( $\Delta CC$  with steps of 1% from  $\pm 0.5\%$ ).

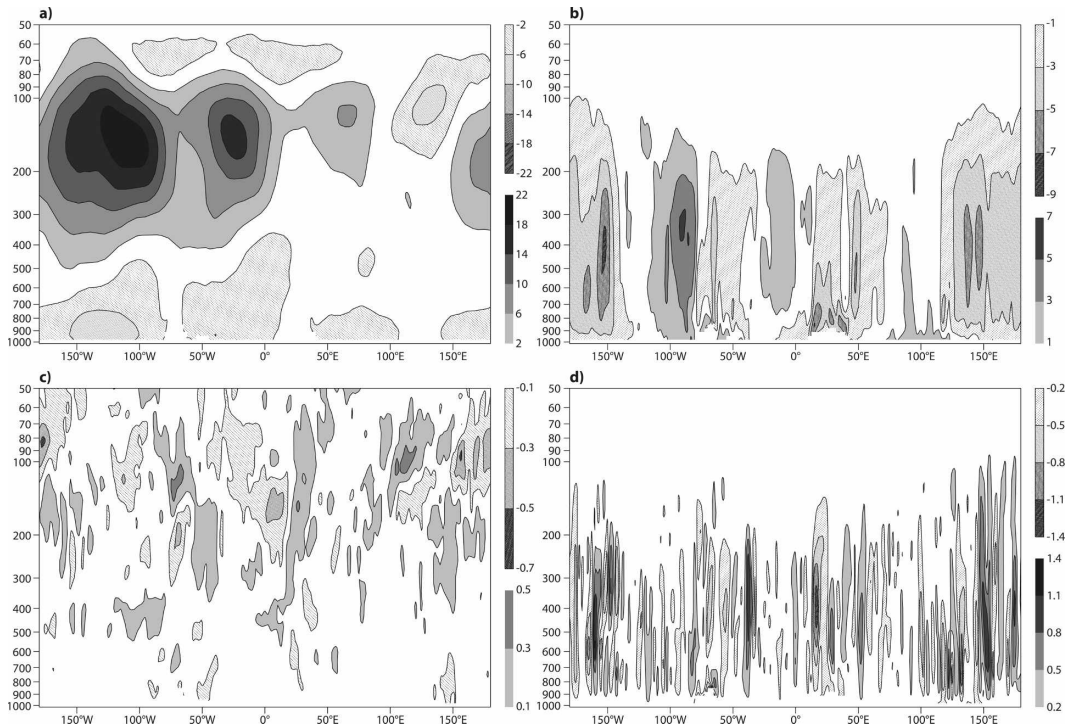


FIG. 14. Atmospheric parameters in the McRad and the 31R2 model for January 2007 in the same conditions as in Fig. 12 for (a), (b) McRad and (c), (d) the differences between McRad and 31R2 for (a), (c) zonal wind and (b), (d) vertical velocity. In (a) are steps of  $3 \text{ m s}^{-1}$  from  $-3 \text{ m s}^{-1}$  for easterlies and steps of  $5 \text{ m s}^{-1}$  from  $5 \text{ m s}^{-1}$  for westerlies. In (b) are steps of  $0.02 \text{ Pa s}^{-1}$  from  $\pm 0.01 \text{ Pa s}^{-1}$ . In (c) are steps of  $0.2 \text{ m s}^{-1}$  from  $\pm 0.1 \text{ m s}^{-1}$ . In (d) are steps of  $0.04 \times 10^{-1} \text{ Pa s}^{-1}$  from  $\pm 0.02 \times 10^{-1} \text{ Pa s}^{-1}$ .

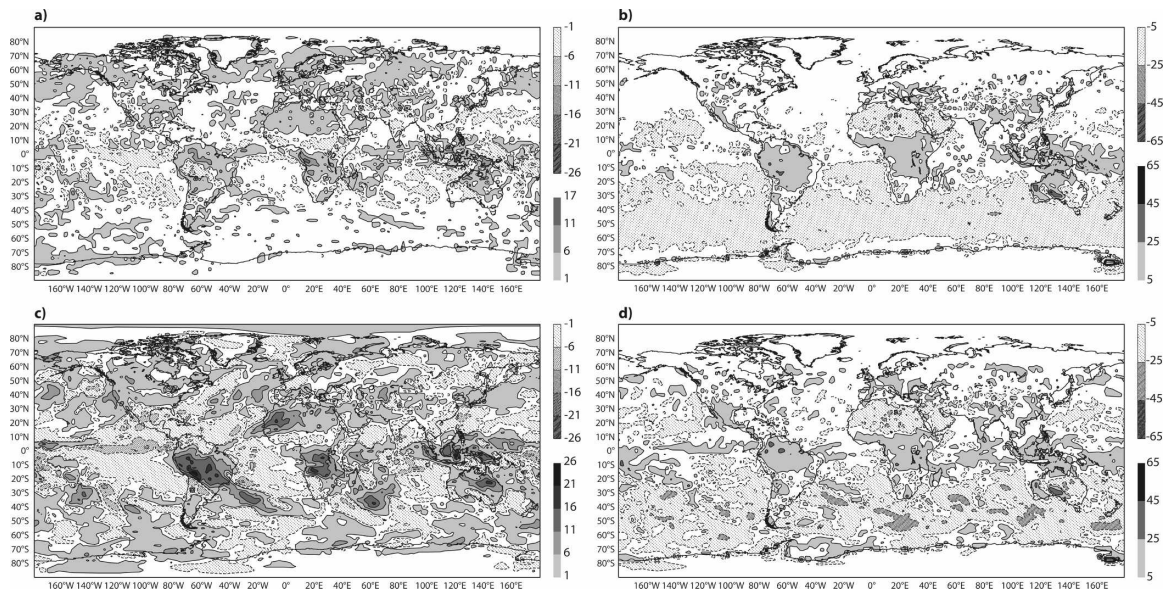


FIG. 15. The difference ( $\text{W m}^{-2}$ ) in (a), (c) OLR and (b), (d) absorbed shortwave radiation at the TOA between the McRad and the 31R2 models for January 2007. (a), (b) The average over the first 24 h and (c), (d) the last 24 h of the 10-day forecasts.

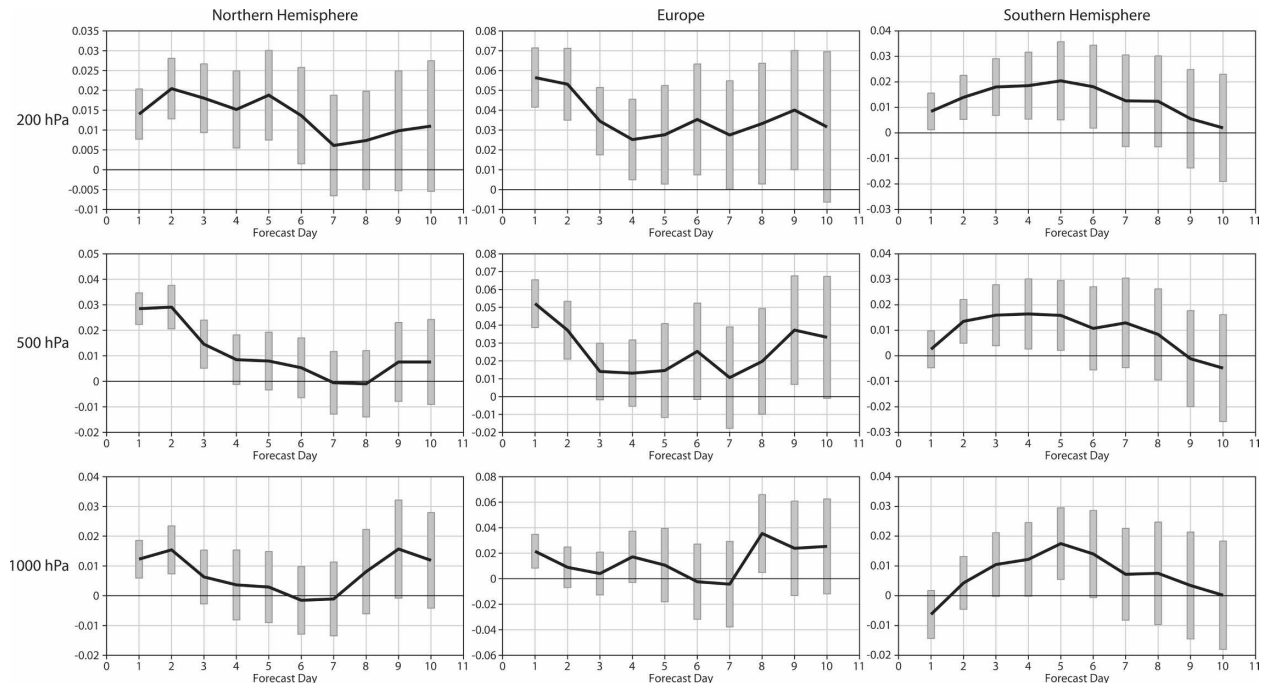


FIG. 16. The time series of the difference in rmse on the geopotential ( $\text{m}^2 \text{s}^{-2}$ ) in the (left) Northern Hemisphere, (middle) European area, and (right) Southern Hemisphere at (top)–(bottom) 200, 500, and 1000 hPa over the period 1 Dec 2006–30 Apr 2007. A value above the zero line denotes an improvement of the McRad forecasts with respect to the operational forecasts.

1000 hPa for the Northern Hemisphere, European area, and Southern Hemisphere, computed over the period 1 December 2006–30 April 2007. A small but systematic improvement is seen over most of the 10 days of the forecasts and for all heights and areas. The improvement in the location of the major tropical cloud systems has a direct impact on the tropical scores, as seen in Fig. 17 for the rmse of the vector wind at four heights within the troposphere and four lead times (after 1, 3, 5, and 7 days in the forecasts).

#### b. Impact on medium-resolution 15-day forecasts as used in the EPS

As discussed in Buizza et al. (1999), for each of the 50 forecast members of the EPS, the model uncertainties deriving from parameterized physical processes are simulated by applying a random number between 0.5 and 1.5 to the sum of the physical tendencies within a  $10^\circ \times 10^\circ$  box over 3 h. The scaled physical tendencies are then passed to the thermodynamic equation to be solved. Therefore, introducing a more approximate treatment of the radiation tendencies (through the use of a more reduced radiation grid) is not likely to deteriorate the quality of the EPS forecasts. Table 4 shows the various radiation resolutions from R255 down to R31 that could be used for the current  $T_L399L62$  EPS configuration.

In 10-day forecasts with McRad running the  $T_L399L62$  model with various resolutions for the radiation grid, the impact on the objective scores was small. For example, Fig. 18 presents the rmse of the temperature at 850 and 200 hPa (the most sensitive parameter) in the tropics for sets of 93 forecasts starting every fourth day, spanning a year from 2 February 2006 to 5 February 2007. For these sets of forecasts with the resolution of the radiation grid being reduced from R255 to R31, the impact on the geopotential is small and does not appear before day 6 of the forecasts (not shown). Similarly, there is a small impact on the rmse of temperature at 850 and 200 hPa. Only the mean error in temperature at 850 hPa for all areas (Northern and Southern Hemispheres and tropical areas) and the mean error in temperature at 200 hPa in the tropics show a distinct signal. However, the difference between R255 and R31 [i.e., a radiation grid coarsening from  $(0.70^\circ)^2$  to  $(5.625^\circ)^2$ ] is at most 0.06 K, with the resolutions between R255 and R63 being very close to each other and R47 and R31 showing a more undesirable impact. In the tropics, where these differences in temperature between the various radiation grids are the most marked, the impact on the wind is very small (not shown). Therefore, it appears that reducing the radiation grid somewhat could allow for a decreased cost of the EPS, with a rather small effect on its overall quality.

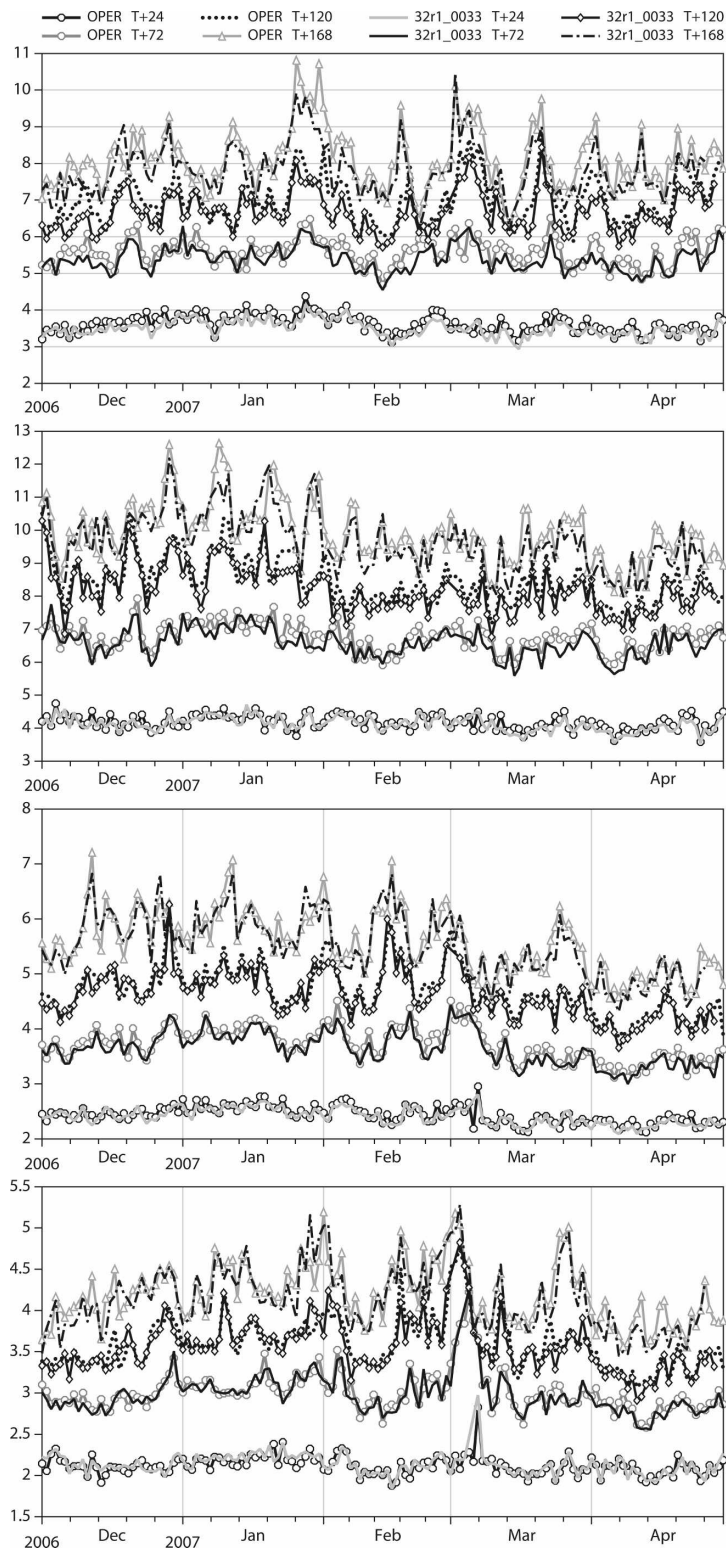


FIG. 17. The time series of the rmse on the vector wind in the tropics (20°N–20°S) at (top)–(bottom) 100, 200, 500, and 850 hPa during the period 1 Dec 2006–30 Apr 2007.

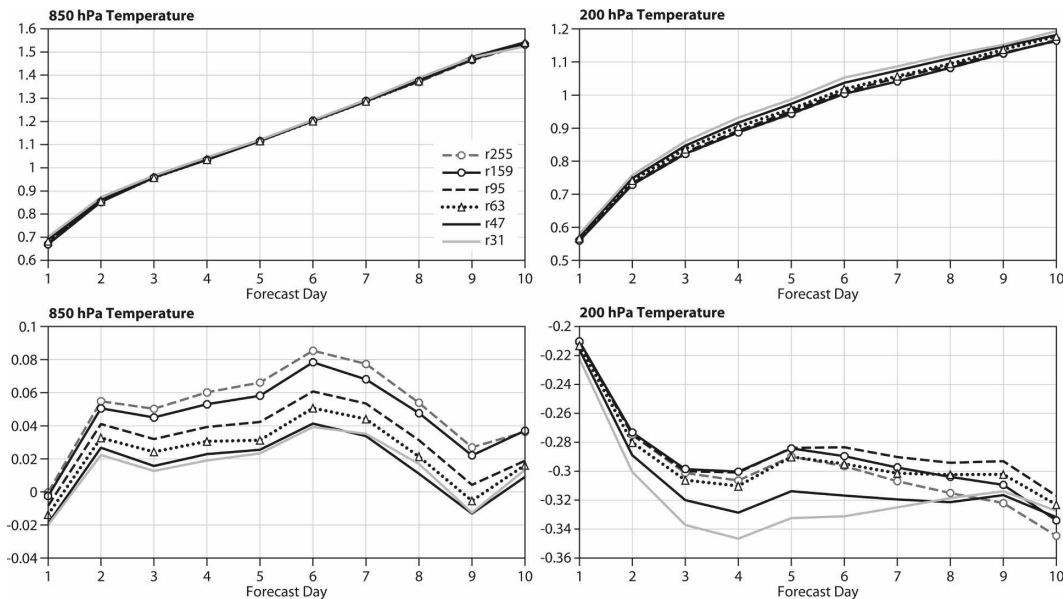


FIG. 18. The (a), (b) rmse and (c), (d) mean error of the temperature at (a), (c) 850 and (b), (d) 200 hPa for McRad 10-day forecasts at  $T_L399L62$ , started every 96 h from 1200 UTC 2 Feb 2006 to 1200 UTC 5 Feb 2007, and using the six different radiation grids from R255 to R31 given in Table 4.

Further tests were conducted within the Variable Resolution Ensemble Prediction System (VAREPS) system, running for 10 days at  $T_L399$  and then at  $T_L255$  for the last five days using three sets of radiation grids: R159/R95, R95/R63, and R47/R31, respectively. Ensemble forecasts were started every two days between 3 December 2006 and 2 January 2007 (16 cases). As shown in Fig. 19, R47/R31 indeed produces an obvious deterioration of the ranked probability skill score of the temperature at 850 hPa in the Southern Hemisphere. The EPS, operational since 5 June 2007, is therefore run at  $T_L399L62R95$  and then at  $T_L255L62R63$ .

## 5. Conclusions and perspectives

The new radiation package McRad presented in this paper became operational with model CY32R2 on 5 June 2007. As with some previous versions of the ECMWF radiation schemes, McRad will be the radiation scheme that will be used in future reanalyses. Consequently, this paper is aimed at documenting its main impact on various configurations of the ECMWF IFS.

McRad includes a new shortwave radiation scheme, revised cloud optical properties, the MODIS-derived land surface albedo, the McICA approach to radiation transfer in cloudy atmospheres, and a more extensive use of a flexible radiation grid that can be made coarser for all applications; however, it is particularly useful when the highest accuracy of the radiative heating

rates, as with the EPS, is not essential for the application.

The impact of McRad was studied in seasonal simulations and 10-day forecasts, and it was shown to benefit the representation of most parameters at both short and longer time scales, relative to the previous operational version of the RT schemes. McRad was shown to improve the signatures of the clouds on the top of the atmosphere radiation budget, in terms of their amplitude and their location. McRad modifies the relative vertical distributions of the longwave and shortwave radiative heating and the amount of shortwave radiation reaching the surface. These changes directly impact the structure of the planetary boundary layer (seen in the change in low-level cloudiness) and the strength of the convection (seen in the change in outgoing longwave radiation and precipitation). By allowing more convection over the tropical continents, McRad indirectly modifies the large-scale Hadley and Ferrel circulation, as seen in the changes in low-level wind over the tropical oceans. All these changes mostly improve the behavior of the model at both short and longer time scales. At short time scales, the McRad forecasts are in better agreement than the operational forecasts, with respect to their own analyses, as seen in the reduced rmse in geopotential and wind.

With respect to surface albedo, the MODIS-derived land surface albedo is currently not used for ice-covered Greenland and Antarctica. By the same token,

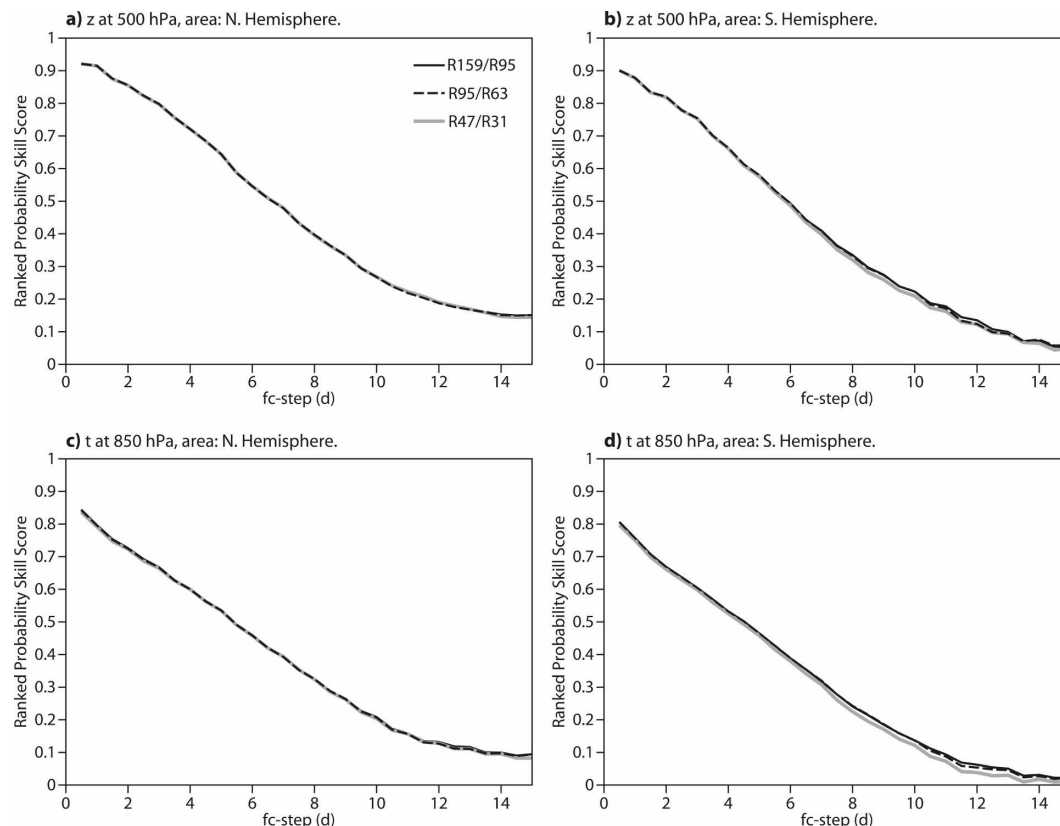


FIG. 19. The ranked probability skill score for the (a), (b) geopotential at 500 and (c), (d) temperature at 850 hPa for the (a), (c) Northern and (b), (d) Southern Hemispheres for the 32R2 EPS, with three sets of radiation grids: R159/R95 (black curve), R95/R63 (dashed curve), and R47/R31 (gray curve).

the definition of the sea ice albedo has not been revised. A revision of the albedo over these areas will be considered in the future.

Up to this point in the paper,  $RRTM_{SW}$  has been advocated as a scheme that is very suitable for the McICA approach because of the large number of spectral computations. However,  $RRTM_{SW}$  has its own merits. With the McRad package, both the LW and SW radiation schemes are based on the same line-by-line model and the same database of spectroscopic parameters. As part of the Atmospheric Radiation Measurement Program of the U.S. Department of Energy, both the  $RRTM_{LW}$  and  $RRTM_{SW}$  models [and the corresponding LBLRTM (Clough et al. 1992; Clough and Iacono 1995)] have been extensively used these last three or four years for sustained comparisons against spectrometer measurements at the ARM Southern Great Plains (SGP), North Slope of Alaska (NSA) and two tropical west Pacific sites. When profiles of the quantities governing the radiation transfer are taken from measurements, the agreement between 1-h averaged, computed and observed radiation fluxes at both top and bottom of the atmosphere is better than 2 W

$m^{-2}$  in LW and 10  $W m^{-2}$  in SW in clear-sky/aerosol-only conditions and 5  $W m^{-2}$  and 25  $W m^{-2}$ , respectively, in cloudy conditions, which is at least a factor of 5 better than the best RT schemes at the end of 1990s.

In terms of methodology, McICA is the most important change because it simplifies the radiation transfer schemes by suppressing all references to partial cloud cover, avoids separate calculations for clear-sky and cloudy parts of the layers, and gets rid of the inherent complexity of the vertical integration, which accounts for the overlapping of these clear and cloudy quantities (reflectances/transmittances, or fluxes). The cloud generator used here (Räisänen et al. 2004), being independent of the radiation transfer, can now handle any overlap situation, and it is used here with a definition of the overlap of cloud layers through decorrelation lengths (Hogan and Illingworth 2000, 2003). It must again be stressed that, through McICA, McRad is ready to handle implicitly any spatial inhomogeneity (horizontal and/or vertical) in the distribution of the condensed water in clouds. The McICA approach could also be used for dealing with inhomogeneities in surface

boundary conditions, a feature that could be of importance when the radiation fluxes are computed over an area encompassing several model grids, each with a number of tiles with different longwave emissivity and shortwave albedo.

McRad will allow the same overlap assumption to be used for radiation transfers and precipitation/evaporation processes, a problem previously solved either only approximately (Jakob and Klein 1999, 2000) or through additional calculations. In the future, McRad will help connect the radiation transfer calculations with cloud information derived from probability density function (PDF)-based cloud schemes [(as that of Tompkins (2002); thanks to the McICA approach] and from observations of the vertical profiles of the condensed water, made available from Cloud-Aerosol Lidar and Infrared Pathfinder Satellite Observation (CALIPSO)-type measurements (thanks to the flexible handling of cloud overlap). As with cloud information, McRad can also include information on the subgrid variability of the water vapor that would be provided by a PDF-based cloud scheme that works on total water.

*Acknowledgments.* A number of other people helped in various aspects of this study: P. Räisänen (FMI) wrote the cloud generator, and E. Mlawer, J. Delamere, and A. Clough (AER, Inc.) originally contributed to the development of the original RRTM longwave and shortwave radiation codes that were later modified to run at ECMWF and that include the McICA approximation to handle cloudiness. MODIS data that were processed in terms of components of the surface albedo were obtained from C. Schaaf at Boston University. At ECMWF, G. Mozdynski originally developed the reduced grid concept and applied it to radiation computations, D. Salmond and J. Hague helped in the debugging and optimizing of various codes, S. Serrar helped implement the MODIS albedo, M. Leutbecher ran the EPS experiments and discussed the results, and A. Weisheimer and F. Doblas-Reyes ran the integrations with the coupled ocean model; P. Bougeault, M. Miller, and A. Beljaars are thanked for their comments on this paper. Author R. Pincus's work was supported by the Office of Science (BER) and by U.S. Department of Energy Grants DE-FG02-03ER63561.

#### REFERENCES

- Barker, H. W., G. L. Stephens, and Q. Fu, 1999: The sensitivity of domain-averaged solar fluxes to assumptions about cloud geometry. *Quart. J. Roy. Meteor. Soc.*, **125**, 2127–2152.
- , R. Pincus, and J.-J. Morcrette, 2002: The Monte-Carlo Independent Column Approximation: Application within large-scale models. *Extended Abstracts, GCSS-ARM Workshop on the Representation of Cloud Systems in Large-Scale Models*, Kananaskis, AB, Canada, GEWEX, 1–10 pp. [Available online at <http://www.met.utah.edu/skrueger/gcss-2002/Extended-Abstracts.pdf>.]
- , and Coauthors, 2003: Assessing 1D atmospheric solar radiative transfer models: Interpretation and handling of unresolved clouds. *J. Climate*, **16**, 2676–2699.
- Buizza, R., M. J. Miller, and T. N. Palmer, 1999: Stochastic representation of model uncertainties in the ECMWF Ensemble Prediction System. *Quart. J. Roy. Meteor. Soc.*, **125**, 2887–2908.
- Cahalan, R. F., W. Ridgway, W. J. Wiscombe, and T. L. Bell, 1994: The albedo of fractal stratocumulus clouds. *J. Atmos. Sci.*, **51**, 2434–2455.
- Cairns, B., A. A. Lacis, and B. E. Carlson, 2000: Absorption within inhomogeneous clouds and its parameterization in general circulation models. *J. Atmos. Sci.*, **57**, 700–714.
- Clough, S. A., and M. J. Iacono, 1995: Line-by-line calculation of atmospheric fluxes and cooling rates. 2. Application to carbon dioxide, ozone, methane, nitrous oxide and the halocarbons. *J. Geophys. Res.*, **100**, 16 519–16 536.
- , —, and J.-L. Moncet, 1992: Line-by-line calculations of atmospheric fluxes and cooling rates: Application to water vapor. *J. Geophys. Res.*, **97**, 15 761–15 786.
- , M. W. Shephard, E. J. Mlawer, J. S. Delamere, M. J. Iacono, K. Cady-Pereira, S. Boukabara, and P. D. Brown, 2005: Atmospheric radiative transfer modeling: A summary of the AER codes. *J. Quant. Spectrosc. Radiat. Transfer*, **91**, 233–244.
- Da Silva, A. M., and S. Levitus, 1994: *Algorithms and procedures*. Vol. 1, *Atlas of Surface Marine Data*. NOAA Atlas NESDIS 6, 83 pp.
- Ebert, E. E., and J. A. Curry, 1992: A parametrization of ice cloud optical properties for climate models. *J. Geophys. Res.*, **97**, 3831–3836.
- Fouquart, Y., 1987: Radiative transfer in climate models. *Physically-Based Modelling and Simulation of Climate and Climatic Changes*. M. E. Schlesinger, Ed., NATO ASI Series, Kluwer Academic, 223–284.
- and B. Bonnel, 1980: Computations of solar heating of the earth's atmosphere: A new parameterization. *Beitr. Phys. Atmos.*, **53**, 35–62.
- , —, and V. Ramaswamy, 1991: Intercomparing shortwave radiation codes for climate studies. *J. Geophys. Res.*, **96**, 8955–8968.
- Fu, Q., 1996: An accurate parameterization of the solar radiative properties of cirrus clouds for climate studies. *J. Climate*, **9**, 2058–2082.
- , P. Yang, and W. B. Sun, 1998: An accurate parameterization of the infrared radiative properties of cirrus clouds of climate models. *J. Climate*, **11**, 2223–2237.
- Geleyn, J.-F., 1977: A comprehensive radiation scheme designed for fast computation. ECMWF Research Department Internal Rep. 8, 36 pp.
- , and A. Hollingsworth, 1979: An economical analytical method for the computation of the interaction between scattering and line absorption of radiation. *Beitr. Phys. Atmos.*, **52**, 1–16.
- Hogan, R. J., and A. J. Illingworth, 2000: Deriving cloud overlap statistics from radar. *Quart. J. Roy. Meteor. Soc.*, **126**, 2903–2909.
- , and —, 2003: Parameterizing ice cloud inhomogeneity and the overlap of inhomogeneities using cloud radar data. *J. Atmos. Sci.*, **60**, 756–767.

- Iacono, M. J., J. S. Delamere, E. J. Mlawer, M. W. Shepard, S. A. Clough, and W. D. Collins, 2008: Radiative forcing by long-lived greenhouse gases: Calculations with the AER radiative transfer models. *J. Geophys. Res.*, **113**, D13103, doi:10.1029/2008JD009944.
- Jakob, C., and S. A. Klein, 1999: The role of vertically varying cloud fraction in the parametrization of microphysical processes in the ECMWF model. *Quart. J. Roy. Meteor. Soc.*, **125**, 941–965.
- , and —, 2000: A parametrization of the effects of cloud and precipitation overlap for use in general circulation models. *Quart. J. Roy. Meteor. Soc.*, **126**, 2525–2544.
- Lacis, A. A., and V. Oinas, 1991: A description of the correlated  $k$  distribution method for modeling nongray gaseous absorption, thermal emission, and multiple scattering in vertically inhomogeneous atmospheres. *J. Geophys. Res.*, **96D**, 9027–9063.
- Li, J., 2002: Accounting for unresolved clouds in a 1D infrared radiative transfer code. Part I: Solution for radiative transfer, including cloud scattering and overlap. *J. Atmos. Sci.*, **59**, 3302–3320.
- Lindner, T. H., and J. Li, 2000: Parameterization of the optical properties for water clouds in the infrared. *J. Climate*, **13**, 1797–1805.
- Martin, G. M., D. W. Johnson, and A. Spice, 1994: The measurement and parameterization of effective radius of droplets in warm stratocumulus. *J. Atmos. Sci.*, **51**, 1823–1842.
- Mlawer, E. J., S. J. Taubman, P. D. Brown, M. J. Iacono, and S. A. Clough, 1997: Radiative transfer for inhomogeneous atmospheres: RRTM, a validated correlated- $k$  model for the longwave. *J. Geophys. Res.*, **102**, 16 663–16 682.
- Morcrette, J.-J., 1990: Impact of changes to the radiation transfer parameterizations plus cloud optical properties in the ECMWF model. *Mon. Wea. Rev.*, **118**, 847–873.
- , 1991: Radiation and cloud radiative properties in the ECMWF operational weather forecast model. *J. Geophys. Res.*, **96**, 9121–9132.
- , 1993: Revision of the clear-sky and cloud radiative properties in the ECMWF model. *ECMWF Newsletter*, No. 61, Reading, United Kingdom, 3–14.
- , 2000: On the effects of the temporal and spatial sampling of radiation fields on the ECMWF forecasts and analyses. *Mon. Wea. Rev.*, **128**, 876–887.
- , 2002a: Assessment of the ECMWF model cloudiness and surface radiation fields at the ARM-SGP site. *Mon. Wea. Rev.*, **130**, 257–277.
- , 2002b: The surface downward longwave radiation in the ECMWF forecast system. *J. Climate*, **15**, 1875–1892.
- , and Y. Fouquart, 1986: The overlapping of cloud layers in shortwave radiation parameterizations. *J. Atmos. Sci.*, **43**, 321–328.
- , and C. Jakob, 2000: The response of the ECMWF model to changes in cloud overlap assumption. *Mon. Wea. Rev.*, **128**, 1707–1732.
- , S. A. Clough, E. J. Mlawer, and M. J. Iacono, 1998: Impact of a validated radiative transfer scheme, RRTM, on the ECMWF model climate and 10-day forecasts. ECMWF Tech. Memo. 252, 47 pp.
- , E. J. Mlawer, M. J. Iacono, and S. A. Clough, 2001: Impact of the radiation transfer scheme RRTM in the ECMWF forecasting system. *ECMWF Newsletter*, No. 91, Reading, United Kingdom, 2–9.
- Oreopoulos, L., and H. W. Barker, 1999: Accounting for subgrid-scale cloud variability in a multi-layer 1D solar radiative transfer algorithm. *Quart. J. Roy. Meteor. Soc.*, **125**, 301–330.
- Ou, S. C., and K.-N. Liou, 1995: Ice microphysics and climatic temperature feedback. *Atmos. Res.*, **35**, 127–138.
- Pincus, R., H. W. Barker, and J.-J. Morcrette, 2003: A fast, flexible, approximate technique for computing radiative transfer in inhomogeneous clouds. *J. Geophys. Res.*, **108D**, 4376, doi:10.1029/2002JD003322.
- Räsänen, P., and H. W. Barker, 2004: Evaluation and optimization of sampling errors for the Monte Carlo Independent Column Approximation. *Quart. J. Roy. Meteor. Soc.*, **130**, 2069–2085.
- , G. A. Isaac, H. W. Barker, and I. Gultepe, 2003: Solar radiative transfer for stratiform clouds with horizontal variations in liquid water path and droplet effective radius. *Quart. J. Roy. Meteor. Soc.*, **129**, 2135–2149.
- , H. W. Barker, M. Khairoutdinov, J. Li, and D. A. Randall, 2004: Stochastic generation of subgrid-scale cloudy columns for large-scale models. *Quart. J. Roy. Meteor. Soc.*, **130**, 2047–2067.
- Schaaf, C. B., and Coauthors, 2002: First operational BRDF, albedo nadir reflectance products from MODIS. *Remote Sens. Environ.*, **83**, 135–148.
- Sellers, P. J., S. O. Los, C. J. Tucker, C. O. Justice, D. A. Dazlich, G. J. Collatz, and D. A. Randall, 1996: A revised land surface parameterization (SiB2) for Atmospheric GCMs. Part II: The generation of global fields of terrestrial biophysical parameters from satellite data. *J. Climate*, **9**, 706–737.
- Senior, C. A., 1999: Comparison of mechanisms of cloud-climate feedbacks in GCMs. *J. Climate*, **12**, 1480–1489.
- Slingo, A., 1989: A GCM parameterization for the shortwave radiative properties of water clouds. *J. Atmos. Sci.*, **46**, 1419–1427.
- Slingo, J. M., 1987: The development and verification of a cloud prediction scheme for the ECMWF model. *Quart. J. Roy. Meteor. Soc.*, **113**, 899–928.
- Smith, E. A., and L. Shi, 1992: Surface forcing of the infrared cooling profile over the Tibetan plateau. Part I: Influence of relative longwave radiative heating at high altitude. *J. Atmos. Sci.*, **49**, 805–822.
- Stephens, G. L., 1988: Radiative transfer through arbitrarily shaped optical media: Part I: A general method of solution. *J. Atmos. Sci.*, **45**, 1818–1836.
- Sun, Z., 2001: Reply to comments by Greg M. McFarquhar on 'Parameterization of effective sizes of cirrus-cloud particles and its verification against observations.' *Quart. J. Roy. Meteor. Soc.*, **127A**, 267–271.
- Tegen, I., P. Hoorig, M. Chin, I. Fung, D. Jacob, and J. Penner, 1997: Contribution of different aerosol species to the global aerosol extinction optical thickness: Estimates from model results. *J. Geophys. Res.*, **102**, 23 895–23 915.
- Tiedtke, M., 1993: Representation of clouds in large-scale models. *Mon. Wea. Rev.*, **121**, 3040–3061.
- , 1996: An extension of cloud-radiation parameterization in the ECMWF model: The representation of subgrid-scale variations of optical depth. *Mon. Wea. Rev.*, **124**, 745–750.
- Tompkins, A. M., 2002: A prognostic parameterization for the subgrid-scale variability of water vapor and clouds in large-scale models and its use to diagnose cloud cover. *J. Atmos. Sci.*, **59**, 1917–1942.
- Uppala, S. M., and Coauthors, 2005: The ERA-40 Re-Analysis. *Quart. J. Roy. Meteor. Soc.*, **131**, 2961–3012.